

# My, how you've grown: a practical guide to modeling size transitions for Integral Projection Model (IPM) applications

Tom E.X. Miller<sup>\*a</sup> and Stephen P. Ellner<sup>b</sup>

<sup>a</sup>Department of BioSciences, Rice University, Houston, TX

<sup>b</sup>Department of Ecology and Evolutionary Biology, Cornell University,  
Ithaca, New York

**Running header:** Better growth modeling for IPMs

---

\*Corresponding author. Department of BioSciences, Rice University, Houston, TX 77005-1827. Email:  
tom.miller@rice.edu Phone: 713-348-4218

<sup>1</sup> **Abstract**

- <sup>2</sup> 1. Integral Projection Models (IPMs) are widely used for studying the dynamics of  
<sup>3</sup> continuously size-structure populations. IPMs require a growth sub-model that  
<sup>4</sup> describes the probability of future size conditional on current size. Over the past  
<sup>5</sup> two decades, most IPM studies have assumed that this probability is normally-  
<sup>6</sup> distributed, despite repeated calls for non-Gaussian approaches that accommodate  
<sup>7</sup> skewness and kurtosis known to occur in size transition data.
- <sup>8</sup> 2. We provide a general workflow for modeling size transitions that accommodates  
<sup>9</sup> non-Gaussian growth patterns while retaining the desirable features (ecologically  
<sup>10</sup> important covariates and random effects) that Gaussian approaches typically pro-  
<sup>11</sup> vide. Our approach emphasizes visual diagnostics of residuals from pilot Gaussian  
<sup>12</sup> models and quantile-based metrics of skewness and kurtosis that vet the fit of the  
<sup>13</sup> Gaussian distribution and guide the selection of an alternative, if necessary. We  
<sup>14</sup> illustrate our methods by reanalyzing size transition data from our published IPM  
<sup>15</sup> studies, targeting a diversity of demographic quantities including population growth  
<sup>16</sup> rate, invasion wave velocity, and evolutionarily stable life history strategies.
- <sup>17</sup> 3. Across one coral and three plant case studies, skewness and excess kurtosis were  
<sup>18</sup> common features of size transition data and non-Gaussian growth models consis-  
<sup>19</sup> tently generated simulated data that were more consistent with the real data than  
<sup>20</sup> pilot Gaussian models. However, in these case studies, the effects of “improved”  
<sup>21</sup> growth modeling on IPM results were generally modest, and differed in direction or  
<sup>22</sup> magnitude between different outputs from the same model.
- <sup>23</sup> 4. Using tools that were not available when IPMs were first developed, it is now possi-  
<sup>24</sup> ble to fit non-Gaussian models to size transition data without sacrificing ecological  
<sup>25</sup> complexity; our worked examples demonstrate how, including open-access data and  
<sup>26</sup> computing scripts. Doing so, as guided by careful interrogation of the data, will re-  
<sup>27</sup> sult in a model that better represents the population for which it is intended.

<sup>28</sup> **Keywords**

## 29 Introduction

30 Structured demographic models – matrix and integral projection models (MPMs and  
31 IPMs) – are powerful tools for data-driven modeling of population dynamics and via-  
32 bility that are widely used in basic and applied settings. In contrast to MPMs for pop-  
33 ulations with discrete structure (life stage, age class, etc.), IPMs (Easterling et al., 2000)  
34 readily accommodate populations structured by continuous state variables, most com-  
35 monly size. A related innovation of the IPM framework is its emphasis on regression-  
36 based modeling for parameter estimation, which often carries important advantages for  
37 making the most of hard-won data (Ellner et al., 2022).

38 A standard workflow allows ecologists to assemble an IPM from data using famili-  
39 iar statistical tools to describe growth, survival, reproduction, and other demographic  
40 transitions as functions of size (Coulson, 2012; Ellner et al., 2016). The relative ease of  
41 the regression-based approach, accommodating multiple covariates (e.g., environmental  
42 factors, experimental treatments) and complex variance structures (e.g., random effects,  
43 correlated errors), has facilitated a growing body of IPM literature that examines how  
44 biotic or abiotic factors affect population dynamics (e.g., Louthan et al., 2022; Ozgul  
45 et al., 2010; Schultz et al., 2017) and explores the consequences of demographic hetero-  
46 geneity associated with spatial, temporal, and individual variation (e.g., Compagnoni  
47 et al., 2016; Crone, 2016; Plard et al., 2018). The vital rate regressions (or “sub-models”)  
48 are the bridge between the individual-level data and the population-level model and its  
49 predictions; it is important to get them right.

50 Compared to other vital rates, growth is special. The regression sub-models for  
51 survival and reproduction only need to provide a single mean value as functions of  
52 size (we use “size” as the name for whatever continuous variable defines the population  
53 structure, which could instead be immune competence, mother’s weight, etc.). But for  
54 modeling growth, the full probability distribution of subsequent size, conditioned on  
55 initial size, must be defined. This distribution defines the growth ‘kernel’  $G(z', z)$  that  
56 gives the probability density of any future size  $z'$  at time  $t + 1$  conditional on current size  
57  $z$  at time  $t$ . Whenever survival and reproduction are size-dependent, the entire distribu-  
58 tion of size transitions can strongly influence IPM predictions because this distribution  
59 governs how frequently size changes are much greater or much lower than average.

60 The original template for modeling size transitions in IPMs was provided by East-  
61 erling et al. 2000. They first tried simple linear regression, assuming normally dis-  
62 tributed size changes with constant variance. Because the residuals from this regression  
63 exhibited non-constant variance, they used a two-step approach that estimated the size-

64 dependence in the residual variance (better options soon became available, such as the  
65 `lme` function in R). However, even after accounting for non-constant variance, growth  
66 data may still deviate from the assumption that size transitions are normally distributed.  
67 Size transitions are often skewed such that large decreases are more common than large  
68 increases (Peterson et al., 2019; Salguero-Gómez and Casper, 2010), or vice versa (Stub-  
69 berud et al., 2019). Size transitions may also exhibit excess kurtosis ('fat tails'), where  
70 extreme growth or shrinkage is more common than predicted by the tails of the normal  
71 distribution (Hérault et al., 2011).

72 The observation that the normal distribution may poorly describe size transitions  
73 in real organisms has been made before, and several studies have emphasized that al-  
74 ternative distributions should be explored (Easterling et al., 2000; Peterson et al., 2019;  
75 Rees et al., 2014; Williams et al., 2012). Nonetheless, default use of Gaussian growth  
76 distributions (often with non-constant variance) remains the standard practice. The gen-  
77 eral state-of-the-art in the literature appears to remain where it was 20 or so years ago,  
78 using the default model without pausing to examine critically whether or not it actually  
79 provides a good description of the data. We are guilty of this, ourselves.

80 The persistence of Gaussian growth modeling is understandable. There is a long  
81 tradition of statistical modeling built on the assumption of normally distributed resid-  
82 uals with constant variance. Popular packages such as `lme4` (Bates et al., 2007), `mgcv`  
83 (Wood, 2017), and `MCMCglmm` (Hadfield et al., 2010) make it easy to fit growth models  
84 with potentially complex fixed- and random-effect structures, but the possible distribu-  
85 tions of continuous responses are limited, and default to Gaussian. Abandoning these  
86 convenient tools for the sake of more flexible growth modeling means, it may seem,  
87 sacrificing the flexibility to rigorously model diverse and potentially complex sources of  
88 variation in growth, some of which may be the motivation driving the study in the first  
89 place.

90 The question we address here is: how can ecologists escape the apparent trade-off  
91 between realistically capturing the variance, skew, and kurtosis of size transition data  
92 on the one hand, and flexibly including the multiple covariates and random effects that  
93 often have substantial impacts on demographic rates? In this article, we offer an answer.

94 Our goal here is to present and illustrate a general and practical "recipe" that moves  
95 growth modeling past the standards set over 20 years ago, using software tools available  
96 now.<sup>1</sup> Like any recipe, users may need to make substitutions or add ingredients to  
97 suit their situation. Our approach emphasizes graphical diagnostics for developing and

---

<sup>1</sup>Our statements about what is available now are based on what tools reliably deliver in our experience, not on what they promise.

98 evaluating growth models, rather than a process centered on statistical model selection.  
99 Through a set of empirical case studies we demonstrate how a simple workflow, using  
100 tools that were nonexistent or not readily available when IPMs first came into use, makes  
101 it straightforward and relatively easy to identify when the default model is a poor fit to  
102 the data, and to then choose and fit a substantially better growth model that is no harder  
103 to use in practice. We illustrate our approach by revisiting published IPM analyses that  
104 assumed Gaussian growth, including our own previous work. In each case, the Gaussian  
105 assumption does not stand up to close scrutiny. We illustrate how we could have done  
106 better, and the consequences of “doing better” for our ecological inferences. All of our  
107 analyses may be reproduced from code and data that are publicly available (see Data  
108 accessibility statement).

## 109 A workflow for growth modeling

110 The modeling workflow that we suggest runs as follows (Fig. 1):

- 111 1. *Fit a “pilot” model or models assuming a Gaussian distribution, but allowing for non-*  
112 *constant variance.*

113 This step is familiar to most IPM users, as it is the start and end of the traditional  
114 workflow. A well-fitted Gaussian model accurately describes the mean and variance  
115 of future size conditional on current size and possibly on other measured covari-  
116 ates or random effects. This step may include model selection to identify which  
117 treatment effects or environmental drivers affect the mean and/or variance of future  
118 size. Non-constant variance is often fitted in a two-stage process, first fitting mean  
119 growth assuming constant variance, then doing a regression relating the squared  
120 residuals to initial size or the fitted mean of subsequent size. Fitting mean and  
121 variance simultaneously, as can be done with R packages **mrgcv** and **nmle**, is ad-  
122 vantageous when possible because incorrectly assuming constant variance can affect  
123 model selection for the mean. But two-step fitting may be convenient when there  
124 are multiple fixed and random effects that can affect growth variance, because the  
125 fitted mean value implicitly accounts for all of them. We illustrate both one-step and  
126 two-step approaches in the case studies below.

127 Allowing non-constant variance removes the need for transforming the data to  
128 stabilize the growth variance. Transformation remains an option when it does not  
129 create new problems (see Discussion), and it may have advantages besides variance

130 stabilization. In particular log-transformation is often appropriate for size data (Ell-  
131 ner et al., 2016), and it helps to avoid eviction at small sizes.

- 132 2. *Use statistical and graphical diagnostics to identify if and how the standardized residuals*  
133 *deviate from Gaussian, and to identify a more appropriate distribution.*

134 If the Gaussian pilot model is valid, the set of standardized residuals (standardized  
135 by the standard deviation) should be Gaussian with mean zero and unit variance,  
136 with no skew or excess kurtosis. This criterion provides a straightforward test for  
137 whether to accept a Gaussian growth model or explore alternatives. If the standard-  
138 ized residuals are satisfactorily Gaussian, skip to the final step of the workflow.

139 There are many ways that growth data may deviate from Gaussian, and the na-  
140 ture of those deviations can guide the search for a better distribution. Frequentist  
141 tests such as the D'Agostino test of skewness (D'Agostino, 1970) and the Anscombe-  
142 Glynn test of kurtosis (Anscombe and Glynn, 1983) could be used to diagnose  
143 whether the aggregate distribution of standardized residuals deviates from normal-  
144 ility (R package **moments** (Komsta and Novomestky, 2015)). However, the aggregate  
145 distribution of standardized residuals may be misleading if properties such as skew  
146 and kurtosis vary with size or other covariates. For example, a change in the di-  
147 rection of skewness from small to large sizes might produce zero overall skewness,  
148 but really requires a distribution flexible enough to accommodate both positive and  
149 negative skew, such as the skewed normal or Johnson  $S_U$  distributions. Alterna-  
150 tively, growth data may lack skew but may exhibit leptokurtosis (in which case the  $t$   
151 distribution may be a good choice) or may shift from platykurtosis to leptokurtosis  
152 depending on initial size (in which case the power exponential distribution may be  
153 a good choice). It is therefore essential to visualize trends in distribution properties  
154 with respect to size, either initial size (for simple models with only size-dependence)  
155 or expected future size (for models with multiple fixed effects). In the case studies  
156 below, we rely on quantile regression of the standardized residuals to visualize skew  
157 and kurtosis as continuous functions of initial size or expected future size. Fig. 1  
158 includes guidance on how the skew and kurtosis properties of the standardized  
159 residuals suggest options for an appropriate growth distribution. In our case stud-  
160 ies we take advantage of the many distributions provided in the **gamlss** R package  
161 (Stasinopoulos et al., 2007), but any other distributions with the necessary properties  
162 can be used.

- 163 3. *Refit the growth model using the chosen distribution.*

164 In models with multiple covariates and/or random effects, each potentially affecting

several distribution parameters (location, scale, skew, kurtosis) in different ways, “refit the model” could entail a massive model selection process to identify the “right” or “best” non-Gaussian model. And with so many options, model uncertainty may be overwhelming and over-fitting becomes a significant risk even if precautions against it are taken. We therefore argue for adopting the more modest goal of remedying any evident defects in the Gaussian model. As we demonstrate below, the functional forms for the mean and standard deviation (or location and scale parameters) can often be carried over from the pilot Gaussian model into a non-Gaussian distribution, leaving skew and kurtosis as the targets for improvement.

Our recommendation for this step is based on the fact that parameter estimation using Gaussian regression models is generally robust to deviations from normality (Schielzeth et al., 2020), meaning that the mean of the Gaussian model is probably a good proxy for the mean of the non-Gaussian model (and if it is not, the next step in the workflow would catch that). The functional forms for skew and kurtosis of the non-Gaussian model can be guided by the qualitative features of the graphical diagnostics (e.g., skewness switches from positive to negative with size).

4. *Test the final model through graphical diagnostics comparing simulated and real growth data.* A good model will generate simulated data that look like the real data. Again, it is important to inspect the properties of simulated data conditional on initial size or expected future size, rather than examining the aggregate distribution. We provide examples below of informative comparisons between simulated and real data, based mainly on quantiles. If the simulated data do not correspond well with real data, alternative (possibly more flexible) growth distributions should be explored, or more complex functions relating distribution parameters to current size and other covariates. However, we again caution against a full-blown model selection exercise. Instead, alternative models should be chosen to remedy observable discrepancies between real and simulated size transition data, and at most slightly modified based on final diagnostics and statistical tests.

## How should skewness and kurtosis be measured?

Improvement of a Gaussian model will involve scrutiny of skewness and kurtosis, so measurement of these properties warrants some attention. The standard measures of skewness and kurtosis (tail thickness) are based on the third and fourth central moments,



**Figure 1:** General workflow of recommendations for IPM growth modeling (left) and guide to common non-Gaussian distributions of size  $x$  for  $x \in \mathbb{R}$  that can accommodate different combinations of skewness and kurtosis (right). All of these distributions (often including multiple versions or parameterizations of each) are available in the package `gamlss.dist`, except for the skewed generalized  $t$ , which is available in the package `sgt` (Davis, 2015).

197 respectively, of the distribution:

$$198 \quad \text{Skewness} = \frac{m_3}{\sigma^3}, \quad \text{Excess kurtosis} = \frac{m_4}{\sigma^4} - 3 \quad (1)$$

199 where  $m_k = \mathbb{E}(X - \bar{X})^k$  is the  $k^{th}$  central moment of a random quantity  $X$  and  $\sigma^2$  is the  
200 variance (second central moment). A Gaussian distribution has zero skewness and zero  
201 excess kurtosis.

202 The standard measures are easy to calculate but their use for choosing and eval-  
203 uating growth models is hindered by their poor sampling properties. Because empirical  
204 estimates involve high powers of data values, a few outliers can produce very inaccurate  
205 estimates. Figure 2 shows a simulated example, where the underlying “data” are a sam-

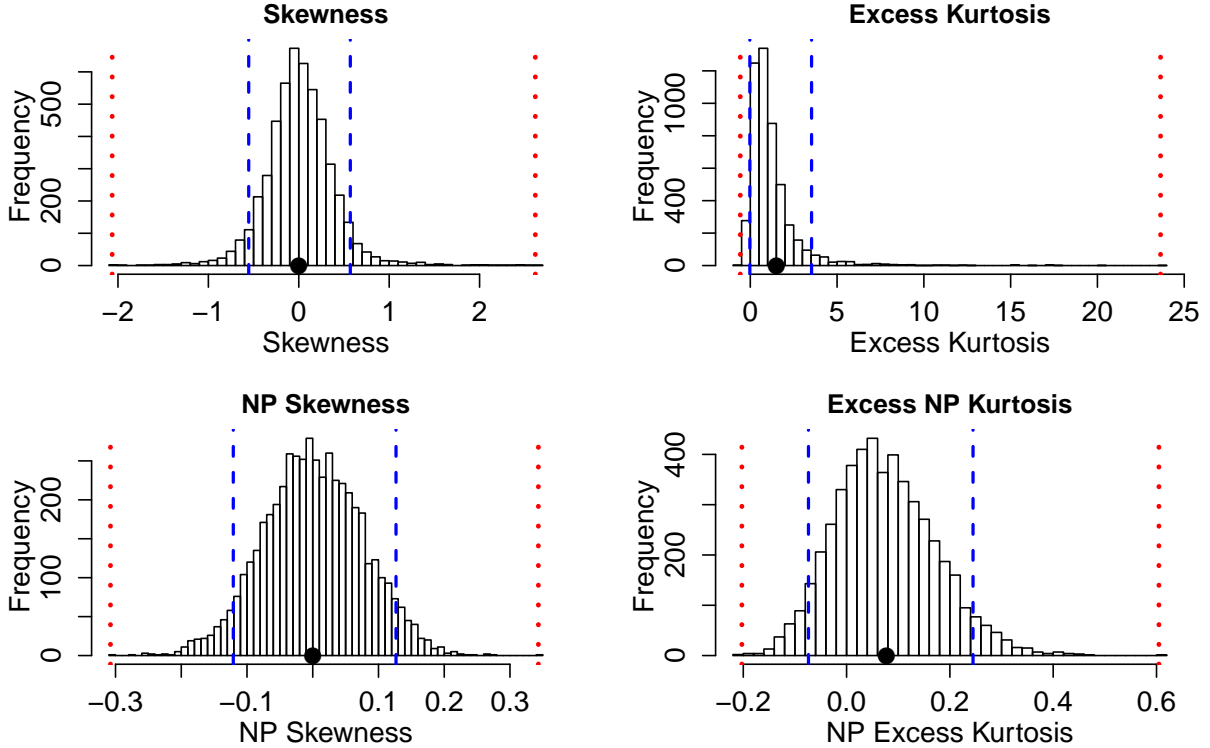


**Figure 2:** Histograms of skewness and kurtosis estimates using moment-based definitions (top two panels), compared with the nonparametric measures based on quantiles (bottom two panels). Note the very large differences in scale. Histograms are based on 5000 replicate draws of a sample of 200 independent values, from a  $t$  distribution with 8 degrees of freedom. Dotted red vertical lines mark the minimum and maximum of sample estimates, and dashed blue lines show the 5th and 95th percentiles. The true value is indicated by a black dot on the  $x$ -axis. Figure drawn by script `NPmoments.R`

ple of size 200 from a  $t$  distribution with 8 degrees of freedom; the true skew is 0, and the true excess kurtosis is 1.5. The distance between the largest and smallest estimates (indicated by the dotted red vertical lines), relative to the distance between the 5th and 95th percentiles, shows the broad extent of extreme values that can occur even with a large sample, especially for kurtosis.

We therefore use nonparametric (NP) measures of skew and kurtosis that are based on quantiles and thus are less sensitive to a few extreme values. Let  $q_\alpha$  denote the  $\alpha$  quantile of a distribution or sample (e.g.,  $q_{0.05}$  is the 5th percentile). For any  $0 < \alpha < 0.5$ , a quantile-based measure of skewness is given by (McGillivray, 1986)

$$\text{NP Skewness} = \frac{q_\alpha + q_{1-\alpha} - 2q_{0.5}}{q_{1-\alpha} - q_\alpha}. \quad (2)$$

216 NP Skewness measures the asymmetry between the tails of the distribution above and  
 217 below the median. The size of the upper tail can be measured (for any  $0 < \alpha < 0.5$ ) by  
 218  $\tau_U = q_{1-\alpha} - q_{0.5}$ ; for  $\alpha = 0.05$  this is the difference between the 95th percentile and the  
 219 median. The lower tail size is  $\tau_L = q_{0.5} - q_\alpha$ . The definition above is equivalent to

$$220 \quad \text{NP Skewness} = \frac{\tau_U - \tau_L}{(\tau_U + \tau_L)}. \quad (3)$$

221 An NP Skewness of  $\pm 0.2$  says that the difference in tail sizes is 20% of their total. The  
 222 range of possible values is -1 to 1. Both  $\alpha = 0.25$  (sometimes called “Kelly’s skewness”) and  
 223  $\alpha = 0.1$  (“Bowley’s skewness”) are common choices. We used  $\alpha = 0.1$ , unless  
 224 otherwise stated.

225 An analogous quantile-based measure of kurtosis (Jones et al., 2011) is

$$226 \quad \text{NP Kurtosis} = \frac{q_{1-\alpha} - q_\alpha}{q_{0.75} - q_{0.25}}. \quad (4)$$

227 For  $\alpha = 0.05$ , NP Kurtosis is the difference between the 95th and 5th percentiles, relative  
 228 to the interquartile range. To facilitate interpretation, we scale NP Kurtosis relative to  
 229 its value for Gaussian distribution, and subtract 1 so that the value for a Gaussian is  
 230 zero. We call this “NP Excess Kurtosis”. The value for a Gaussian distribution is zero. A  
 231 value of  $\pm 0.2$  means that the tails are on average 20% heavier (or lighter) than those of  
 232 a Gaussian with the same interquartile range. We calculate NP Kurtosis using  $\alpha = 0.05$   
 233 unless otherwise stated, to focus on the tail edges, but again this is somewhat arbitrary.

234 Figure 2C,D illustrate how, applied to exactly the same simulated samples, the non-  
 235 parametric measures produce a smaller fraction of highly inaccurate estimates caused  
 236 by a few extreme values in the sample. But also note that, in contrast to the moment-  
 237 based measures, numerically small values of the nonparametric measures (e.g., 0.1 or 0.2)  
 238 should not be disregarded, because they are both scaled so that a value of 1 indicates  
 239 extremely large departures from a Gaussian distribution.

240 Quantile-based estimation of skewness and kurtosis carries the added value that  
 241 quantile regression methods may be used to derive these properties of size transitions  
 242 as continuous functions of initial size or expected future size. In the examples below,  
 243 we sometimes use the **qgam** package to fit smooth additive quantile regression models,  
 244 which have the flexibility to accommodate nonlinear size-dependence in skewness and  
 245 kurtosis. One risk of a gam-based approach is that fitted quantiles may be too “wiggly”  
 246 without constraints on their complexity. In the examples below, we limit complexity by  
 247 fitting splines with  $k = 4$  or  $k = 6$  basis functions. For the gam-averse, other quantile  
 248 regression models may be equally suitable, and we illustrate those, too. For consistency

249 with nonparametric skewness and kurtosis, in comparisons of real and simulated data  
 250 below, we use quantile-based measures of location and scale, and use quantile regression  
 251 to visualize these as functions of size. Specifically, following Wan et al. (2014),

$$252 \quad \text{NP Mean} = \frac{q_{0.25} + q_{0.5} + q_{0.75}}{3} \quad (5)$$

253 and

$$254 \quad \text{NP SD} = \frac{q_{0.75} - q_{0.25}}{1.35}. \quad (6)$$

## 255 1 Case study: lichen, *Vulpicida pinastri*

256 We begin with a simple example where current size is the only predictor of future size.  
 257 Growth data for the epiphytic lichen *Vulpicida pinastri* were first analyzed by Shriner et  
 258 al. 2012 and analyzed again by Peterson et al. 2019 in their study of negatively skewed  
 259 growth distributions. We therefore had an *a priori* expectation of deviation from normal-  
 260 ity. The authors of the original study used a mixture distribution that separated “normal  
 261 growth or shrinkage” from “extreme shrinkage”. We aimed to fit a single, flexible growth  
 262 model that could realistically accommodate both types of size transition without requir-  
 263 ing *ad hoc* decisions about which observations of shrinkage were “extreme” or not. The  
 264 data set includes 1,542 inter-annual transitions in thallus area ( $cm^2$ ) observed from 2004  
 265 to 2009 in Kennicott Valley, AK.

266 With initial size as the only predictor, a simple way to fit a Gaussian model with  
 267 nonconstant variance is the `gam` function in `mgcv` library (Wood, 2017) using the `gaulss`  
 268 family. Following a bit of model selection, we fit the mean and standard deviation of  
 269 future size as second-order polynomials of current size, then derived the scaled residuals  
 270 from the fitted mean and sd:

```
271 # XH is the data frame
272 # t0 and t1 are initial and final thallus area, respectively
273 fitGAU <- gam(list(t1 ~ t0 + I(t0^2), ~ t0 + I(t0^2)), data=XH, gamma=1.4, family=gaulss)
274 XH$fitted_mean = predict(fitGAU, type="response")[,1]
275 XH$fitted_sd <- 1/predict(fitGAU, type="response")[,2]
276 XH$scaledResids=residuals(fitGAU, type="response")/XH$fitted_sd
```

277 Quantile regression on the scaled residuals generates the diagnostics shown in Fig. 3  
 278 (see script `Vulpicida_IPMS.R`). As expected based on previous analyses, visual analysis  
 279 of the standardized residuals indicated negative skew, especially at larger sizes (Fig. 3B).  
 280 We also find positive excess kurtosis for all sizes.

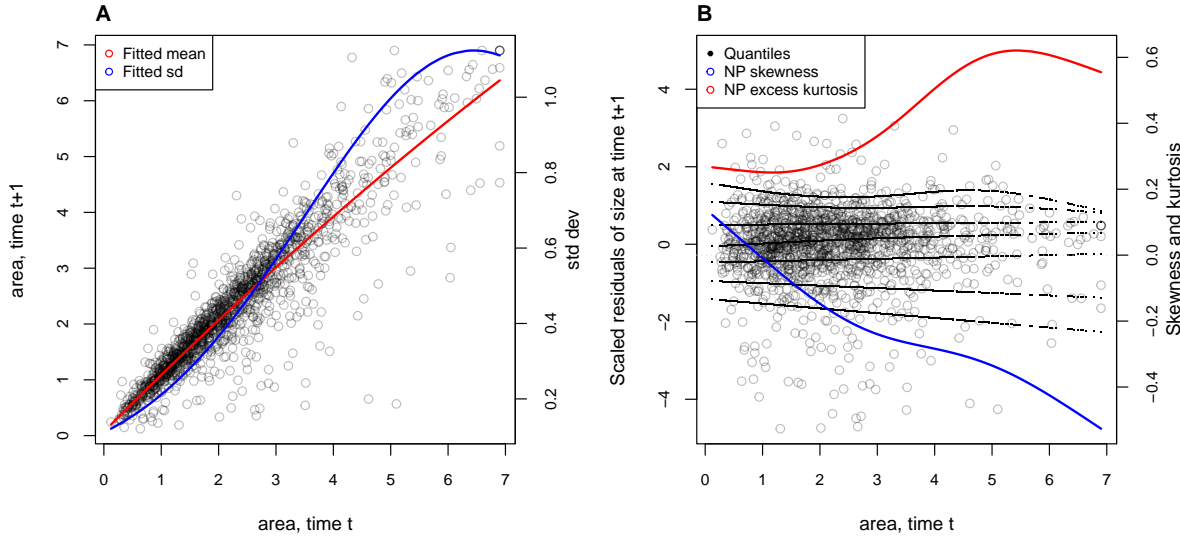


**Figure 3:** **A**, Size transition data for lichens, *Vulpicida pinastri*, and fitted gam with mean (red) and standard deviation (blue) of future size conditional on current size. **B**, Quantile regressions of scaled residuals on size and nonparametric estimates of skewness (red) and excess kurtosis (blue) derived from them. Black lines in **B** show the 5th, 10th, 25th, 50th, 75th, 90th, and 95th quantiles. Figure made by script `Vulpicida_IPMS.R`.

Lacking clear evidence of size-dependence in kurtosis, we turned to the Johnson's *S-U* (JSU) distribution for improvement. The JSU is a four-parameter, leptokurtic distribution that can accommodate positive or negative skew; it also has the convenient property that parameters `mu` and `sigma` are the mean and standard deviation, respectively, which facilitates a natural correspondence to the pilot Gaussian model. The JSU is not available as a distribution family in any of the standard linear or additive modeling packages, to our knowledge, but that need not be a barrier for this or any other distribution as long as we can write a likelihood function (`dJSU()` is provided by `gamlss`). Following the best-fit Gaussian model, we defined `mu` and `sigma` of the JSU as second-order polynomials of initial size and, based on signals of skewness and kurtosis in the standardized residuals (Fig. 3B), we define parameter `nu` (which controls skewness) as a linear function of size and `tau` (which controls kurtosis) as a positive constant; the likelihood function therefore has nine parameters to estimate. We fit the model using the `maxLik` package and starting values for `mu` and `sigma` based on estimates from the pilot Gaussian model:

```

296  ## define function that returns the JSU negative log-likelihood
297  LogLikJSU=function(pars){
298      dJSU(size_t1,

```

```

299     mu=pars[1]+pars[2]*size_t+pars[3]*size_t^2,
300     sigma=exp(pars[4]+pars[5]*size_t+pars[6]*size_t^2),
301     nu = pars[7]+pars[8]*size_t,
302     tau = exp(pars[9]), log=TRUE)
303 }
304 ## starting parameter values
305 p0<-c(coef(fitGAU22)[1:6],0,0,0)
306 ## fit with maxlik
307 outJSU=maxLik(logLik=LogLikJSU,start=p0*exp(0.2*rnorm(length(p0))),
308 method="BHHH",control=list(iterlim=5000,printLevel=2),finalHessian=FALSE);

```

309 Data simulation from the fitted JSU model indicates a compelling improvement over the  
 310 best Gaussian model, particularly in skewness and kurtosis (Fig. 4).

311 To understand the practical consequences of improved growth modeling, we as-  
 312 sembled the remainder of the lichen IPM following Shriver et al. 2012. The asymptotic  
 313 population growth rate based on Gaussian growth ( $\lambda_{GAU} = 1.001$ ) differs from the JSU  
 314 growth model ( $\lambda_{JSU} = 0.991$ ) by about 1% annual population growth, in line with re-  
 315 sults of Peterson et al. 2019. However, even this modest difference can lead to strongly  
 316 biased estimates of extinction risk from the Gaussian model, particularly over longer  
 317 time horizons (Fig. 5). We also explored differences in other life history metrics (Table).<sup>2</sup>  
 318 For example, the JSU growth model predicts values for mean lifespan, mean lifetime  
 319 reproductive success, and mean age at reproduction that are 19%, 25%, and 14% lower  
 320 than the Gaussian growth model. In this case study, properly modeling non-normal size  
 321 transitions – which was easy to do with a few extra lines of code – can have important  
 322 effects on ecological inferences.

323 One could argue that the lichen data set was a convenient “straw man” to disqualify  
 324 Gaussian growth, since it was recognized by the original and subsequent IPM analysts  
 325 that this species requires a skewed distribution of size transitions (Peterson et al., 2019;  
 326 Shriver et al., 2012). In all remaining case studies, including those in the Appendix,  
 327 we re-examine growth data that were modeled as Gaussian by the data originators in  
 328 published IPM studies.

---

<sup>2</sup>What is the best way to cite Chrissy Hernandez' life history functions?

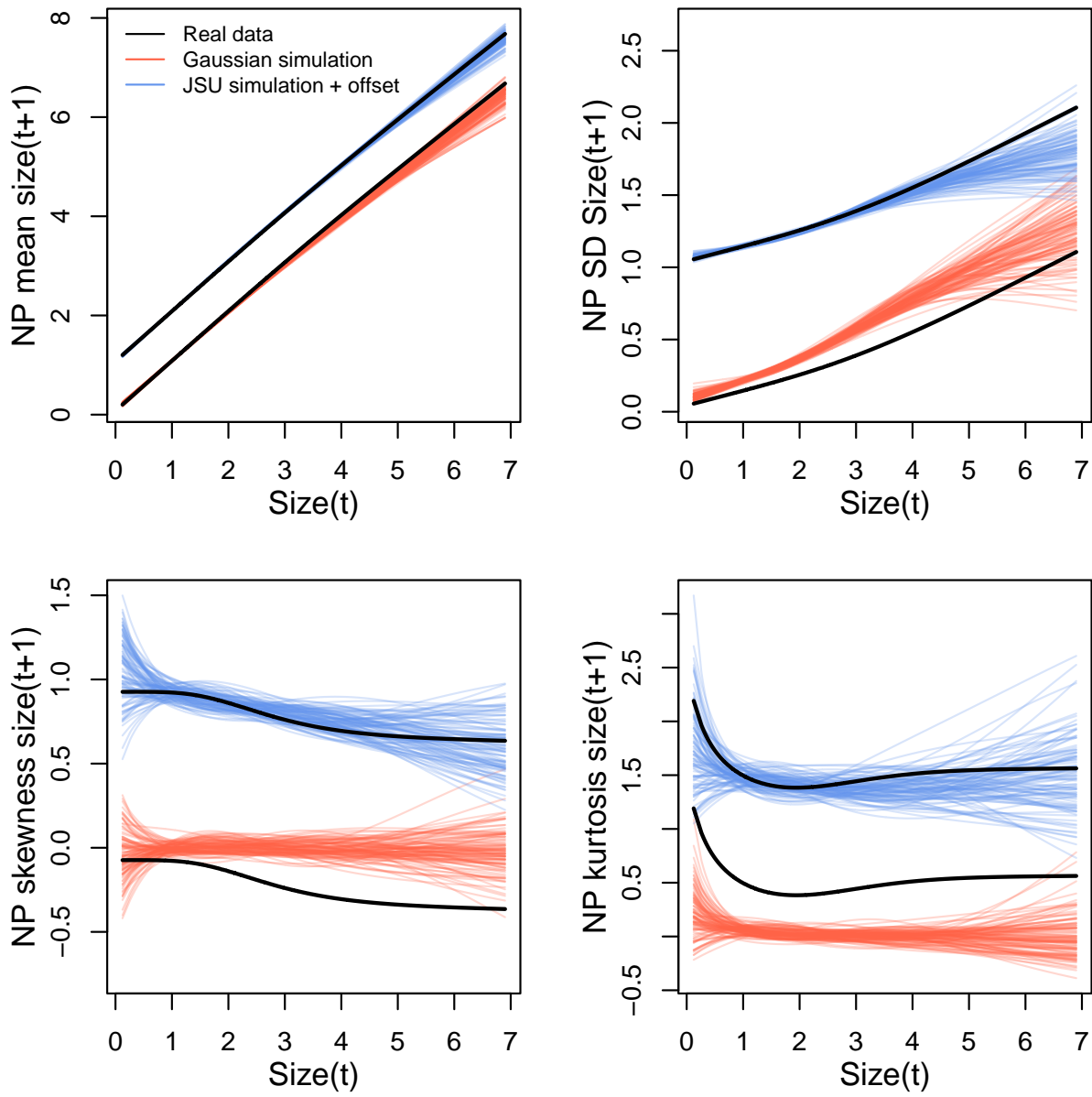


**Figure 4:** Comparisons among real lichen data and data simulated from Gaussian and JSU growth models for NP mean, NP standard deviation, NP skewness, and NP excess kurtosis of future size conditional on current size. Figure made by script `Vuplicida_IPMs.R`.

## 329 2 Case study: tree cholla cactus, *Cylindriopuntia imbricata*

330 The next case study, focusing on the tree cholla cactus *Cylindriopuntia imbricata* at the  
 331 Sevilleta Long-Term Ecological Research site in central New Mexico, adds a new feature  
 332 on top of the simple size-dependent regressions in the previous study: random effects

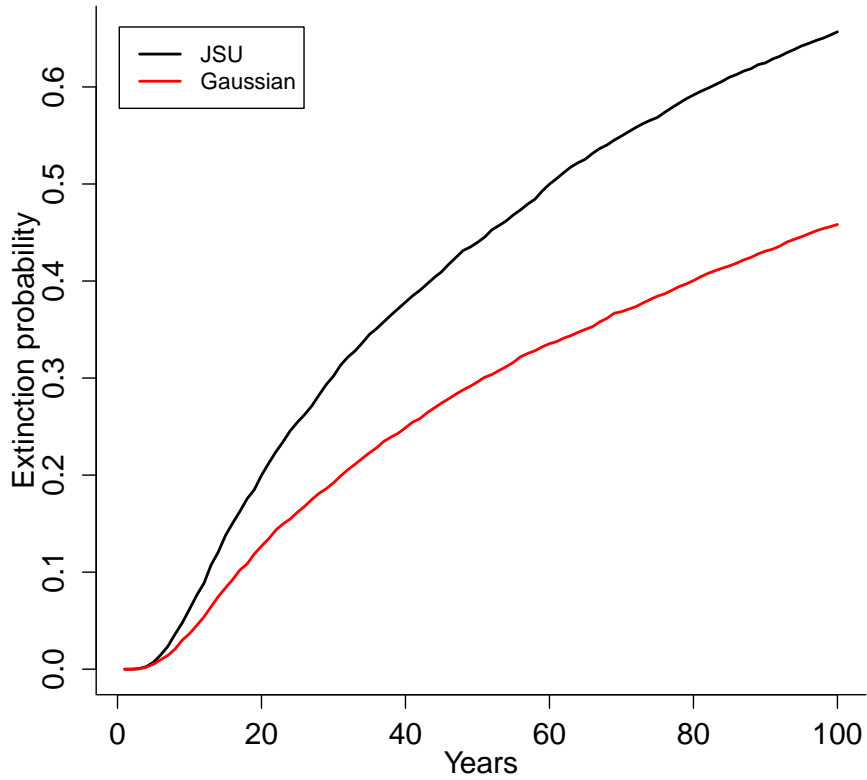


**Figure 5:** Extinction risk estimated from individual-based simulation of IPMs based on Gaussian and Johnson's S-U (JSU) growth distributions. Figure made by script Vuplicida\_IPMs.R.

associated with temporal (year) and spatial (plot) environmental heterogeneity. This long-term study of cactus demography was initiated in 2004 and different subsets of the data have been analyzed in various IPM studies, all using Gaussian growth kernels (Compagnoni et al., 2016; Czachura and Miller, 2020; Elderd and Miller, 2016; Miller et al., 2009; Ohm and Miller, 2014). In fact, (Elderd and Miller, 2016) presented a Gaussian growth model fit to the cactus data as an example of a well fit growth function, based on a marginal distribution of residuals that appeared approximately Gaussian and posterior predictive checks (PPCs) of a Bayesian model that suggested consistency between the real data and data simulated from the fitted model (Fig. 4 in (Elderd and Miller, 2016)). While PPCs and the associated “Bayesian P-value” are popular diagnostic tools, they are often considered to be too conservative (Conn et al., 2018; Zhang, 2014), failing to reject marginally bad models even though they are very effective in rejecting

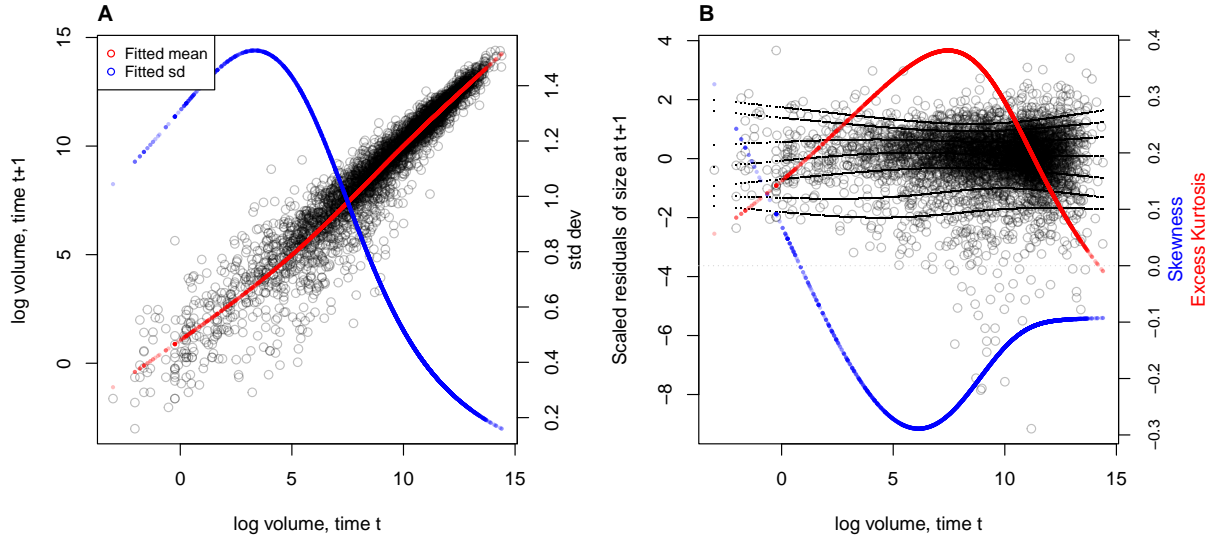


**Figure 6:** **A**, Size transition data for tree cholla cacti, *Cylindropuntia imbricata*, and fitted gam with mean (red) and standard deviation (blue) of future size conditional on current size. **B**, Quantile regressions of scaled residuals on size and nonparametric estimates of skewness (red) and excess kurtosis (blue) derived from them. Black lines in **B** show the 5th, 10th, 25th, 50th, 75th, 90th, and 95th quantiles. Figure made by script `cactus_growth_modeling_qgam.R`.

models that are terrible. The choice of discrepancy function (the statistic used to compare real and simulated data) can also be limiting: in our previous work, we used a discrepancy function focused on variance (the sum of the squared residuals), so we had a built-in blind-spot for mismatches in higher moments. In the clarity of hindsight, the PPC gave a false sense of security; the Gaussian was a poor choice all along.

The data for this new analysis include 4844 size transition observations from 929 individuals spanning 13 transition years (2004–2018) and 11 spatial replicates (three spatial blocks in years 2004–2008 and eight 30m-by-30m plots in years 2009–2018). The data are provided in Miller (2020). Following previous studies, we quantified size as the natural logarithm of plant volume ( $cm^3$ ), derived from height and width measurements.

We begin the growth modeling workflow, as above, with a generalized additive model with the mean and standard deviation of size in year  $t + 1$  modeled as function of size in year  $t$ , with random intercepts for year and plot and assuming normally distributed residuals (`family=gaulss()`). The standardized residuals, accounting for size-dependent residual variance (Fig. 6A), show clear signals of negative skew and positive excess kurtosis across most of the size distribution but strongest in the middle of the size distribution (Fig. 6B).

362 To better capture size transitions, we need a distribution with negative skew and  
 363 positive excess kurtosis, but both of which may be negligible at some sizes. We first tried  
 364 Johnson's  $S_U$  and then the skewed  $t$  distributions, both of which are limited to positive  
 365 excess kurtosis. Both distributions provided some improvement over the Gaussian, but  
 366 were not happy with the fit of either. Iterating through the workflow (Fig. 1), we arrived  
 367 at the SHASH distribution, which is more flexible than either the JSU or skewed  $t$ , capa-  
 368 ble of capturing a greater range of kurtosis for a given amount of skew, and vice versa  
 369 (Jones and Pewsey (2009); Appendix S.1). Furthermore, fitting the SHASH as a general-  
 370 ized additive model with **mgcv** allowed for flexible, non-monotonic size-dependence in  
 371 skewness and kurtosis without the need for model selection on specific size-dependent  
 372 functions; through iterations of trial and error, we found this flexibility was necessary  
 373 to generate simulated data that compared favorably to the real data. The other distri-  
 374 butions that we tried are not available as **mgcv** families, so we fit these with custom  
 375 maximum likelihood functions, an approach we illustrate in the next case study. The  
 376 SHASH gam for the cactus data included random intercepts for the location parameter,  
 377 representing spatial and temporal heterogeneity:

```

 378 fit_shash <- gam(list(logvol_t1 ~ s(logvol_t,k=4) +
 379   s(plot,bs="re") + s(year_t,bs="re"), # location
 380   ~ s(logvol_t,k=4), # log-scale
 381   ~ s(logvol_t,k=4), # skewness
 382   ~ s(logvol_t,k=4)), # log-kurtosis
 383   data = CYIM_grow,
 384   family = shash,
 385   optimizer = "efs")
  
```

386 The SHASH model provided good correspondence between simulated and real  
 387 data, and provided more compelling improvement over the Gaussian model than we  
 388 saw in the coral case study (Fig. S-7). The SHASH model over-estimated negative skew  
 389 at some sizes relative to the signal of skewness in the data (Fig. S-7C), but the nature of  
 390 size-dependent skew in the data is not very biologically plausible and may instead be  
 391 driven by the tail-wagging tendency of gams. As in the coral case study, we see that cor-  
 392 rectly modeling skewness and kurtosis improved estimation of the mean and standard  
 393 deviation (Fig. S-7A,B), yielding a growth model that is clearly truer to the data than the  
 394 pilot Gaussian fit.

395 We explored how improved growth modeling influenced IPM results, leveraging  
 396 the plot and year structure of the study design to quantify spatial and temporal vari-

ance in fitness. We used the fitted random effects from the vital rate models to estimate the asymptotic growth rate for each year ( $\lambda_t$ ), centered on the average plot, and for each plot ( $\lambda_p$ ), centered on the average year. This allowed us to quantify demographic variance associated with temporal and spatial heterogeneity. We found that the Gaussian growth model tended to over-estimate  $\lambda_t$ , particularly in the harshest years (Fig. 7A), and thus under-estimated temporal variance in fitness ( $Var(\lambda_{t(Gaussian)}) = 0.0018$ ,  $Var(\lambda_{t(SHASH)}) = 0.0023$ ). The opposite was true for plot-to-plot variation (Fig. 7B), where the Gaussian model under-estimated  $\lambda_p$  and over-estimated spatial variance in fitness ( $Var(\lambda_{p(Gaussian)}) = 0.00015$ ,  $Var(\lambda_{p(SHASH)}) = 0.000088$ ). Across both growth models, fluctuations in fitness were stronger through time than across space. The difference in temporal variance would suggest that Gaussian growth modeling would lead to over-estimation of the stochastic growth rate  $\lambda_S$ , since temporal variance has a negative influence on  $\lambda_S$ . However, this was not the case: stochastic IPMs based on Gaussian and SHASH growth models had nearly identical stochastic growth rates ( $\lambda_S(Gaussian) = 0.9906$ ,  $\lambda_S(Gaussian) = 0.9909$ ). This is likely because temporal fluctuations in vital rates, which is where the SHASH growth model would make a difference, have a weaker influence on  $\lambda_S$  than the temporal fluctuations in size structure that they generate (Compagnoni et al., 2016; Ellis and Crone, 2013). Thus, depending on the target of one's analysis, modeling non-Gaussian size transitions with a Gaussian growth model could bias results in either direction, or make no difference at all.

## 2.1 Case study: lady orchid, *Orchis purpurea*

Our final case study examines selection on life history strategies in the lady orchid *Orchis purpurea*. In a prior study, Miller et al. 2012 contrasted the growth trajectories from year  $t$  to  $t + 1$  for plants that did or did not flower in year  $t$ , as a way to quantify costs of reproduction. The different growth kernels were then used in an IPM to quantify evolutionarily stable life history strategies: the optimal flowering size that balances benefits of waiting to flower at larger sizes against the risk of dying before reaching those sizes. The original study assumed a Gaussian distribution of size transitions and allowed for non-constant variance with respect to initial size. Here we re-visit that analysis applying our growth modeling workflow to derive improved growth kernels for flowering and non-flowering orchids. We use this case study to illustrate several new elements and challenges, including modeling skewness and kurtosis as functions of expected future size (instead of initial size).

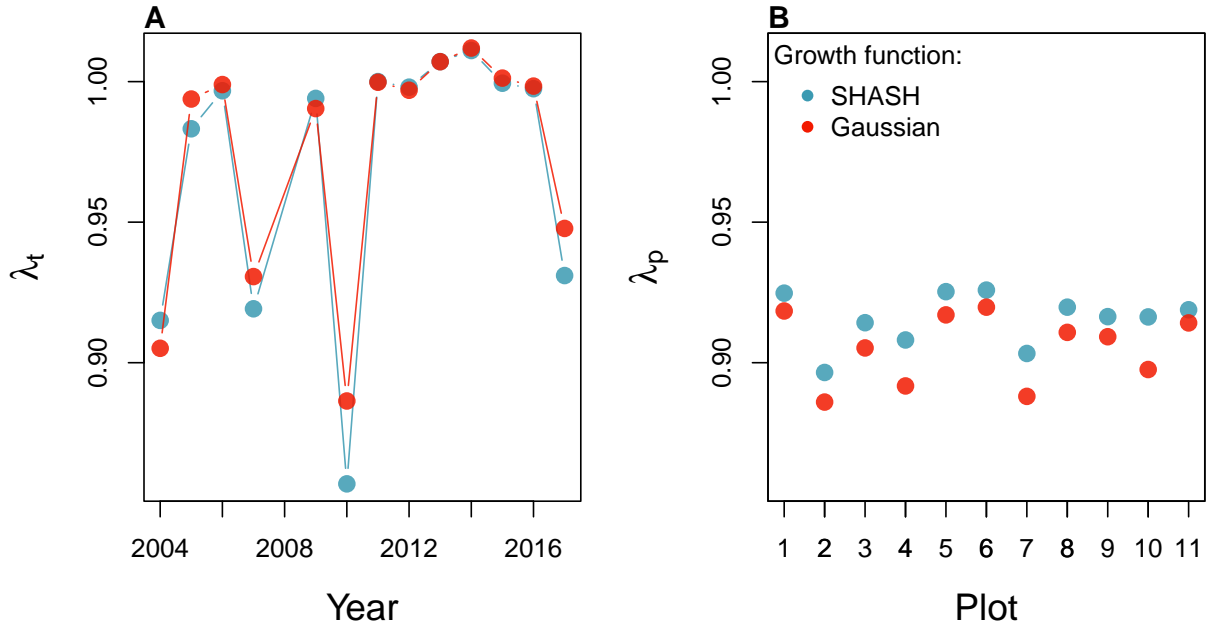


**Figure 7:** Temporal (A) and spatial (B) heterogeneity in fitness for the tree cholla cactus (*Cylindriopuntia imbricata*) predicted by IPMs using Gaussian or SHASH growth models. Figure made by script `cactus_growth_modeling_qgam.R`.

The data, originated by Dr. Hans Jacquemyn and used here with permission, come from 368 plants in a Belgian population that was censused annually from 2003 through 2011 (for this reanalysis we are using data only from the “light” habitat). Size was measured as leaf area ( $cm^2$ ) summed over all leaves, and we analyzed the natural logarithm of total leaf area as the size variable of the IPM.

As a variation on software, our pilot Gaussian approach used the **lme4** package to fit three candidate linear models for size in year  $t + 1$  that included fixed effects of size in year  $t$  (model 1), additive effects of size and flowering status in year  $t$  (model 2), or an interaction between size and flowering (model 3), all including random intercepts for year. The interaction model with strongly favored ( $\Delta AIC = 10.5$ ). Unlike our previous case studies, here we have multiple fixed effects (initial size and flowering status) that may influence the variance of future size. In cases such as this, it is often convenient to model variance as a function of expected future size, rather than initial size as we did with the lichens and cacti. The expected (or “fitted”) values reflect the combined influence of all fixed and random effects, and therefore implicitly account for multiple sources of variation in the variance. While there are several software packages for simultaneously modeling Gaussian mean and variance as functions of independent variables (**mgcv** for gam models as we saw above, **nlme** for linear models), modeling variance as

448 a function of the mean is trickier because they cannot easily be fit simultaneously. Here  
449 we use an iterative re-weighting approach – which is not elegant, but it works.

450 For Gaussian models, weights  $w_i$  can be used to indicate that the observations  $y_i$   
451 vary in their dispersion around the mean. In general, the iterative steps are as follows,  
452 and code to execute these steps may be found in SCRIPT.

1. Fit the expected value and normally-distributed residuals with constant standard deviation  $\sigma$ :

$$y_i = \mu_i + \epsilon_i$$

$$\epsilon_i \sim N(0, \sigma)$$

2. Fit the standard deviation of the residuals as a function of the expected value.

Weights are derived as the inverse of the fitted variance:

$$\epsilon_i \sim N(0, f(\mu_i))$$

$$w_i = 1/f(\mu_i)^2$$

3. Re-fit the observation model, weighting the residual variance according to step 2:

$$y_i = \mu_i + \epsilon_i$$

$$\epsilon_i \sim N(0, \sigma \times \sqrt{w_i})$$

453 We iterated steps 2 and 3 until the weights did not change. In step 2, we modeled the  
454 standard deviation as a second-order polynomial of the expected value ( $\log(f(\mu_i)) =$   
455  $\beta_0 + \beta_1\mu_i + \beta_2\mu_i^2$ ); in exploratory analyses we found that the the second-order term  
456 provided necessary flexibility to fit the standard deviation. We did this for all candidate  
457 models and, for fair AIC comparison, we re-fit all candidate models with the same  
458 weights, estimated from the top model.

459 The updated model selection continued to favor model 3, but now with a weaker  
460 improvement over the next-best model ( $\Delta AIC = 6.7$ ). The best Gaussian model indicated  
461 a growth cost associated with flowering at the start of the census interval and a decline in  
462 growth variance with increasing expected values (Fig. ??A). The standardized residuals  
463 indicated negative skewness (10–20% difference in tail weight) and excess kurtosis (10–  
464 40% fatter than Gaussian) across much of the size distribution but both negligible at  
465 large sizes (Fig. ??B).

466 As improvements, we explored the skewed  $t$  and Johnson's SU distributions, both  
467 leptokurtic distributions with flexible skewness. We were happier with the skewed  $t$ ,

which we fit with a custom likelihood function similar to the JSU growth model fit to the lichen data. However, rather than re-fitting all the parameters of the skewed  $t$  model, here we build a “hybrid” that uses the fitted mean and standard deviation functions from Gaussian pilot model, and estimates the parameters that control skewness and kurtosis as linear functions of predicted future size. This is easy because the **gamlss.dist** package provides a parameterization of the skewed  $t$  in which the location parameter  $\mu$  is the mean and scale parameter  $\sigma$  is the standard deviation (Rigby et al., 2019). The hybrid likelihood looks like this:

```

## log_area_t1 and log_area_t are the size obervations
## GAU_fitted and GAU_sd are mean and standard deviation from best Gaussian
## pars is a vector of free parameters to be estimated
SSTLogLik=function(pars){
  dSST(log_area_t1,
    mu=GAU_fitted,
    sigma=GAU_sd,
    nu = exp(pars[1] + pars[2]*GAU_fitted),
    tau = exp(pars[3] + pars[4]*GAU_fitted)+2,
    log=TRUE)
}

```

Based on diagnostics of the standardized residuals, parameters that control skewness and kurtosis are defined as linear functions of the mean, and those coefficients are estimated by maximum likelihood (note that the tau parameter uses a  $\log(x - 2)$  link function). This approach relies on the robustness of Gaussian models to deviations from normality, which implies that the fitted mean and variance from a Gaussian model are a good approximation for the mean and variance of a corresponding non-Gaussian model. If one is skeptical of this approach, it is possible to simultaneously re-fit all parameters of the skewed  $t$ . However, recall that our pilot Gaussian approach included random effects for year, and therefore the expected values getting passed into dSST account for this source of variation. Coding random effects “from scratch” into a custom likelihood model is possible (we provide guidance on one way to do this, using the “shrinkage” approach, in Appendix XX) but should generally not be necessary. Instead, a key advantage of the hybrid approach is convenient retention of the fitted random effects and associated variance components, which get shuttled from the Gaussian model into the non-Gaussian model without any fuss (it was critical that we used a parameterization of the skewed  $t$  for which `mu` is the mean and `sigma` is the standard deviation). And, if this

503 approach does not “work” (i.e., deviations from normality biased the fitted values of the  
504 Gaussian model) one would quickly find out through the simulation step of the work-  
505 flow. In this case, size transition data simulated from this model corresponded favorably  
506 to the real data, much better than the pilot Gaussian model, including improvements in  
507 the standard deviation, skewness, and kurtosis of future size (Fig. S-8).

508 Finally, we used the improved growth model to revisit key results of the original  
509 study. Miller et al. (2012) used the orchid IPM to estimate the evolutionarily stable strat-  
510 egy (ESS) as the mean size at flowering that maximizes lifetime reproductive success  
511 ( $R_0$ ), given the constraint that flowering when small reduces growth and thus elevates  
512 mortality risk. Repeating that analysis here, we found that improved growth modeling  
513 has virtually no influence on predictions for optimal life history strategies (Fig. 8). ESS  
514 flowering sizes were nearly identical between IPMs with Gaussian vs skewed  $t$  growth  
515 models, and both aligned well with the observed mean flowering size (dashed vertical  
516 line in Fig. 8A). Extending beyond the original study, we also explored expected remain-  
517 ing lifespan for different ages and sizes (R package **Rage** (Jones et al., 2022)). Gaussian  
518 and skewed  $t$  growth models predicted nearly identical mean remaining lifespans across  
519 the stage and size distribution (Fig. 8B). **However, the skewed  $t$  model predicted consis-**  
520 **tently greater variance in remaining lifespan, nearly 10% greater at some sizes.**<sup>3</sup> Thus,  
521 as we have seen in other case studies, the practical consequences of improved growth  
522 modeling depend on what one aims to learn from the IPM.

### 523 3 Discussion

524 Much of the appeal of integral projection models has stemmed from their embrace of  
525 continuous size structure through reliance on regression-based approaches, and the po-  
526 tentially complex fixed- and random-effect structures that these approaches allow. Using  
527 familiar statistical tools and with relatively few parameters to estimate, IPM users can  
528 incorporate important sources of variation in demography and interrogate their influ-  
529 ence on ecological and evolutionary dynamics. With this opportunity comes the burden  
530 of getting it right: IPMs are good models of the populations they are intended repre-  
531 sent only insofar as the statistical models provide good fits to the underlying data. The  
532 growth sub-model is the trickiest part of “getting it right” because it defines a distri-  
533 bution of future size conditional on current size. Distributions have many properties –

---

<sup>3</sup>*Do not believe this result! I have left it here as a placeholder because I would like to do this correctly. But I think there are problems with Rage's `life_expect_var()` function. The predicted variance declines linearly with matrix dimension.*

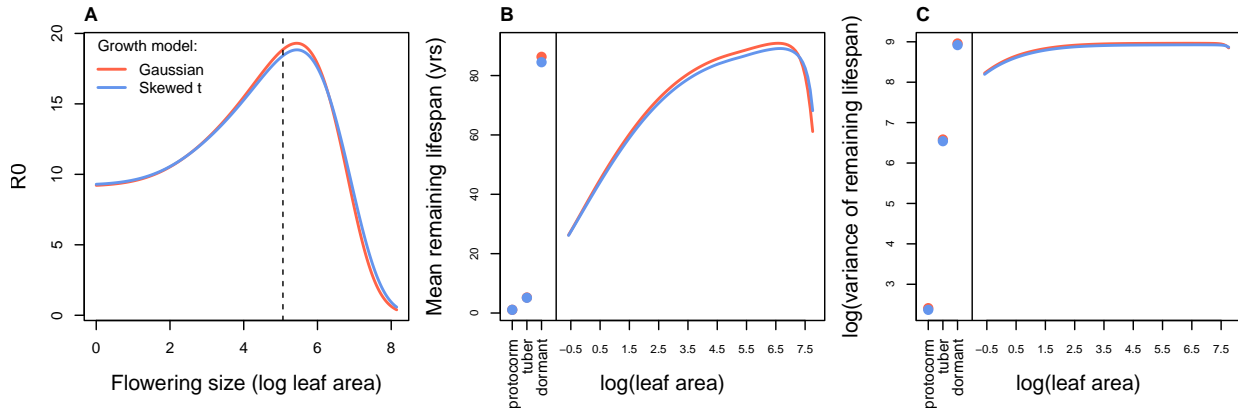


**Figure 8:** Orchid life history results from IPMs using Gaussian or skewed  $t$  growth models. **A**, Lifetime reproductive success ( $R_0$ ) as a function of mean size of flowering. Dashed vertical line shows the observed mean flowering size. **B-C**, Mean and variance of remaining lifespan as a function of size or stage. The orchid IPM includes three discrete below-ground stages (protocorm, tuber, and dormant plant) in addition to continuous size of above-ground plants. **SPE: the variance of lifespan results are now correct, using Chrissy Hernandez's functions instead of RAGE. And the result is, non-Gaussian again has no effect.**

“moments” – and a good growth model should recapitulate the properties of real size transitions. The default assumption of normally distributed size transitions, employed overwhelmingly across 20+ years of IPM studies, is an arbitrary historical precedent. In our case studies (chosen simply because we had the data at our fingertips) and, we suspect, more broadly, skewness and excess kurtosis were common features of size transition data: shrinking was more common than growing, and large changes in size were more common than a Gaussian model would predict. Our most important message is that the standard assumption of normally-distributed size transitions should be abandoned and a more inquisitive process of growth modeling should take its place.

We have attempted to lay out a general workflow for what that process should look like, guided by visual diagnostics of standardized residuals. One implication of relying on visual diagnostics is that goodness of fit is in the eye of the beholder. This approach can empower IPM users to make informed choices, but it is not very prescriptive: we have not suggested any hard rules for when one or another distribution should be used, only that a good growth model should generate data that look like the real thing. Alternatively, model selection could be used to identify best-fitting growth distributions and best-fitting functions for higher moments. However, model selection among growth distributions with 3-5 parameters, each of which may be functions of state variables or fitted values, can quickly explode in complexity, and we are not convinced it is worth

553 the trouble. It should be possible to find a good growth model without worrying about  
554 which one is “best”.

555 Our work follows the important contribution of Peterson et al. 2019, who were  
556 motivated by a similar problem (inadequacy of the Gaussian distribution for skewed  
557 size transitions) but arrived at different recommendations for dealing with the problem.  
558 These authors developed a creative approach in which size data are transformed onto a  
559  $[0, 1]$  scale and then size transitions are modeled using beta regression. The beta distri-  
560 bution can accommodate positive, negative, or zero skew; as Peterson et al. demonstrate,  
561 this approach is a viable option for skewed growth data. However, beta regression also  
562 has some important downsides: common beta regression packages do not fit random  
563 effects(e.g., **betareg** (Cribari-Neto and Zeileis, 2010)) or do not do so reliably (in our ex-  
564 perience **gamlss** is numerically unstable); the two-parameter beta distribution has rigid  
565 mean-variance and skewness-kurtosis relationships that may not describe the data well;  
566 and<sup>4</sup>. Rather than shoe-horn size transition data into a default beta distribution, we find  
567 it more natural and appropriate to leverage the vast arsenal of real-valued probability  
568 distributions – all of them at one’s fingertips with a few lines of code – and let the data  
569 suggest appropriate alternatives based on the residuals of a pilot Gaussian model. The  
570 workflow that we have envisioned requires no sacrifice of complexity in random effects  
571 or covariates for the sake of modeling skewness and kurtosis.

572 While the arsenal of candidate distributions is indeed vast, in our analyses for this  
573 paper, we found ourselves coming back time and again to a few usual suspects. The  
574 four-parameter SHASH distribution, for example, is able to flexibly accommodate inde-  
575 pendent, size-dependent variation in variance, skewness, and kurtosis, and it is available  
576 as a distribution family in the well-developed **mgcv** package. In our case study analy-  
577 ses it was consistently among the top non-Gaussian candidates and was our model of  
578 choice for the coral, cactus, and pike data sets. While we have emphasized the im-  
579 portance of moving away from a single default distribution of size transitions, if one  
580 were to want or need a default distribution (e.g., in software packages for IPM con-  
581 struction [cite IPMpack]) one could do worse than the SHASH. In cases where size  
582 transitions are leptokurtic but consistently so across the size distribution, the Johnson’s  
583 S-U (used for creosotebush) and skewed *t* (used for lady orchid) distributions were easy  
584 to fit with custom likelihood functions. All of the distributions we have used (and  
585 the specific parameterizations we have implemented) share the property that their lo-  
586 cation and scale parameters correspond to the mean and standard deviation, which  
587 is not essential but it facilitates interpretation and an intuitive connection to the pilot

---

<sup>4</sup>Steve, I recall you have a beef with transformation to  $[0,1]$ , so that would go here.

588 Gaussian model. The five-parameter skewed generalized  $t$  (sgt) generalizes many other  
589 real-valued distributions (cite) and is therefore another flexible option, but it does not  
590 share the location=mean and scale=sd property, and in our experience can be hard to fit.  
591 Finally, finding an appropriate non-Gaussian alternative does not solve all the problems  
592 of growth modeling. “Eviction” from the approximating matrix of the IPM kernel is an  
593 ever-present danger and requires vigilance to detect and correct (Williams et al., 2012).

594 In all of our case studies, non-Gaussian growth models always yielded more sat-  
595 isfying fits to size transition data than the Gaussian models published in those papers.  
596 However, much to our relief, none of these re-analyses yielded a “gotcha” result that  
597 overturned results of the original study. In this small sampling of case studies, improved  
598 growth modeling had weak to modest effects on IPM results, similar in magnitude to  
599 the results of Peterson et al. (2019). We caution against taking too much comfort in this  
600 outcome; we can imagine other scenarios in which the choice of the growth distribution  
601 could be more consequential. It is worth noting that most of our case studies focused on  
602 perennial life histories (perennial plants, corals, lichens), characterized by relatively slow  
603 growth, heavy losses during recruitment, and high survival once established. Life cycles  
604 such as these may be relatively robust to subtle features of the growth kernel. More  
605 systematic comparative analyses may provide insight into which types of species and  
606 life histories are more likely to exhibit strong skewness and kurtosis, and the conditions  
607 under which demographic analysis is more or less sensitive to these features of size trans-  
608 ition. It is also worth noting, as we saw in several case studies, that different outputs  
609 from the same model can be more or less sensitive to the choice of growth distribution.

610 Across our case studies we have attempted to illustrate a diversity of software pack-  
611 ages and computational approaches to model fitting, to reflect the diversity of prefer-  
612 ences and habits that the community of IPM users bring to their own analyses. We like  
613 generalized additive models (gams) for their flexibility and for **mgcv**’s numerous op-  
614 tions for distribution families and overall speed and reliability. However, there are some  
615 applications for which classical parametric regression would be preferable because the  
616 coefficients carry biological meaning. For example, regression coefficients may be tar-  
617 gets of natural selection (Rees and Ellner, 2016) and may combine to influence traits of  
618 interest such as the expected size at flowering (e.g. in Fig. 8A), a function of the intercept  
619 and slope of the size-dependent flowering function (Metcalf et al., 2003). Some poten-  
620 tially useful but relatively obscure distributions may not be available in linear modeling  
621 software packages, but that should not be a barrier to their use: as we have illustrated in  
622 several case studies, custom likelihood functions open up diverse possibilities for non-  
623 Gaussian growth modeling without sacrificing the complex, multi-level features that one

624 might be accustomed to fitting in **lme4**, for example. We have illustrated fitting growth  
625 models using maximum likelihood but Bayesian analysis is another option that may fur-  
626 ther broaden the options of non-Gaussian candidate distributions and may help estimate  
627 hard-to-fit parameters through the brute force of sampling algorithms. Bayesian analy-  
628 sis also provides a natural way to propagate uncertainty from the vital rate sub-models  
629 through the predictions of the IPM (Elderd and Miller, 2016).

630 This paper has focused on size transitions, but IPMs have been increasingly ex-  
631 tended in ways that capture other continuous state variables, and the same problems  
632 and solutions we propose should apply in those cases. For example, IPMs can be used  
633 to model infectious disease dynamics, where hosts may exhibit continuous variation in  
634 infection load (e.g., parasite density), and host vital rate processes depend on infection  
635 load (Metcalf et al., 2016; Wilber et al., 2016). Such models must define probabilities of  
636 future infection load conditional on current load, and would therefore benefit from the  
637 same modeling workflow that we have outlined for size transitions.

### 638 **3.1 Conclusion**

## 639 **Acknowledgements**

640 This research was supported by US NSF grants DEB-1933497 to SPE and DEB-1754468,  
641 2208857, and 2225027 to TEXM.

## 642 **4 Authorship statement**

643 All authors discussed all aspects of the research and contributed to developing methods,  
644 analyzing data, and writing and revising the paper.

## 645 **5 Data accessibility statement**

646 No original data appear in this paper. Should the paper be accepted, all computer scripts  
647 supporting the results will be archived in a Zenodo package, with the DOI included at  
648 the end of the article. During peer review, our data and code are available at [https://github.com/texmiller/IPM\\_size\\_transitions](https://github.com/texmiller/IPM_size_transitions).  
649

650 **Literature Cited**

- 651 Anscombe, F. J. and Glynn, W. J. (1983). Distribution of the kurtosis statistic  $b_2$  for  
652 normal samples. *Biometrika*, 70(1):227–234.
- 653 Bates, D., Sarkar, D., Bates, M. D., and Matrix, L. (2007). The lme4 package. *R package  
654 version*, 2(1):74.
- 655 Bruno, J. F., Ellner, S. P., Vu, I., Kim, K., and Harvell, C. D. (2011). Impacts of aspergillosis  
656 on sea fan coral demography: modeling a moving target. *Ecological Monographs*,  
657 81(1):123–139.
- 658 Compagnoni, A., Bibian, A. J., Ochocki, B. M., Rogers, H. S., Schultz, E. L., Sneck, M. E.,  
659 Elderd, B. D., Iler, A. M., Inouye, D. W., Jacquemyn, H., et al. (2016). The effect of  
660 demographic correlations on the stochastic population dynamics of perennial plants.  
661 *Ecological Monographs*, 86(4):480–494.
- 662 Conn, P. B., Johnson, D. S., Williams, P. J., Melin, S. R., and Hooten, M. B. (2018). A guide  
663 to bayesian model checking for ecologists. *Ecological Monographs*, 88(4):526–542.
- 664 Cooch, E. G. and White, G. C. (2020, accessed 5/17/2020). *Program MARK - a 'gentle  
665 introduction'*. Available at phidot.org.
- 666 Coulson, T. (2012). Integral projections models, their construction and use in posing  
667 hypotheses in ecology. *Oikos*, 121(9):1337–1350.
- 668 Cribari-Neto, F. and Zeileis, A. (2010). Beta regression in r. *Journal of statistical software*,  
669 34:1–24.
- 670 Crone, E. E. (2016). Contrasting effects of spatial heterogeneity and environmental  
671 stochasticity on population dynamics of a perennial wildflower. *Journal of Ecology*,  
672 104(2):281–291.
- 673 Czachura, K. and Miller, T. E. (2020). Demographic back-casting reveals that subtle  
674 dimensions of climate change have strong effects on population viability. *Journal of  
675 Ecology*.
- 676 D'Agostino, R. B. (1970). Transformation to normality of the null distribution of  $g_1$ .  
677 *Biometrika*, pages 679–681.
- 678 Davis, C. (2015). *sgt: Skewed Generalized T Distribution Tree*. R package version 2.0.

- 679 Drees, T., Ochocki, B. M., Collins, S. L., and Miller, T. E. (2023). Demography and  
680 dispersal at a grass-shrub ecotone: a spatial integral projection model for woody plant  
681 encroachment. *Ecological Monographs*, page e1574.
- 682 Easterling, M. R., Ellner, S. P., and Dixon, P. M. (2000). Size-specific sensitivity: applying  
683 a new structured population model. *Ecology*, 81(3):694–708.
- 684 Elderd, B. D. and Miller, T. E. (2016). Quantifying demographic uncertainty: Bayesian  
685 methods for integral projection models. *Ecological Monographs*, 86(1):125–144.
- 686 Ellis, M. M. and Crone, E. E. (2013). The role of transient dynamics in stochastic popula-  
687 tion growth for nine perennial plants. *Ecology*, 94(8):1681–1686.
- 688 Ellner, S. P., Adler, P. B., Childs, D. Z., Hooker, G., Miller, T. E., and Rees, M. (2022).  
689 A critical comparison of integral projection and matrix projection models for demo-  
690 graphic analysis: Comment. *Ecology*, 103(10):e3605.
- 691 Ellner, S. P., Childs, D. Z., and Rees, M. (2016). *Data-driven Modeling of Structured Popula-*  
692 *tions: A Practical Guide to the Integral Projection Model*. Springer, New York.
- 693 Gould, W. R. and Nichols, J. D. (1998). Estimation of temporal variability of survival in  
694 animal populations. *Ecology*, 79:2531 – 2538.
- 695 Gu, C. (2013). *Smoothing Spline ANOVA Models*. Springer Science+Business Media, New  
696 York, 2 edition.
- 697 Hadfield, J. D. et al. (2010). Mcmc methods for multi-response generalized linear mixed  
698 models: the mcmcglmm r package. *Journal of Statistical Software*, 33(2):1–22.
- 699 Hérault, B., Bachelot, B., Poorter, L., Rossi, V., Bongers, F., Chave, J., Paine, C. T., Wagner,  
700 F., and Baraloto, C. (2011). Functional traits shape ontogenetic growth trajectories of  
701 rain forest tree species. *Journal of ecology*, 99(6):1431–1440.
- 702 Jones, M. and Pewsey, A. (2009). Sinh-arcsinh distributions. *Biometrika*, 96:761 – 780.
- 703 Jones, M. C., Rosco, J. F., and Pewsey, A. (2011). Skewness-invariant measures of kurtosis.  
704 *The American Statistician*, 65(2):89 – 95.
- 705 Jones, O. R., Barks, P., Stott, I., James, T. D., Levin, S., Petry, W. K., Capdevila, P., Che-  
706 Castaldo, J., Jackson, J., Römer, G., et al. (2022). Rcompadre and rage—two r pack-  
707 ages to facilitate the use of the compadre and comadre databases and calculation of

- 708 life-history traits from matrix population models. *Methods in Ecology and Evolution*,  
709 13(4):770–781.
- 710 Komsta, L. and Novomestky, F. (2015). Moments, cumulants, skewness, kurtosis and  
711 related tests. *R package version*, 14(1).
- 712 Link, W. A. and Nichols, J. D. (1994). On the importance of sampling variance to inves-  
713 tigations of temporal variation in animal population size. *Oikos*, 69(3):539 – 544.
- 714 Louthan, A. M., Keighron, M., Kiekebusch, E., Cayton, H., Terando, A., and Morris, W. F.  
715 (2022). Climate change weakens the impact of disturbance interval on the growth rate  
716 of natural populations of venus flytrap. *Ecological Monographs*, 92(4):e1528.
- 717 McGillivray, H. (1986). Skewness and asymmetry: measures and orderings. *Annals of  
718 Statistics*, 14:994–1011.
- 719 Metcalf, C. J. E., Ellner, S. P., Childs, D. Z., Salguero-Gómez, R., Merow, C., McMahon,  
720 S. M., Jongejans, E., and Rees, M. (2015). Statistical modelling of annual variation for  
721 inference on stochastic population dynamics using Integral Projection Models. *Methods  
722 in Ecology and Evolution*, 6:1007–1017.
- 723 Metcalf, C. J. E., Graham, A. L., Martinez-Bakker, M., and Childs, D. Z. (2016). Oppor-  
724 tunities and challenges of i ntegral p rojection m odels for modelling host-parasite  
725 dynamics. *Journal of Animal Ecology*, 85(2):343–355.
- 726 Metcalf, J. C., Rose, K. E., and Rees, M. (2003). Evolutionary demography of monocarpic  
727 perennials. *Trends in Ecology & Evolution*, 18(9):471–480.
- 728 Miller, T. E. (2020). Long-term study of tree cholla demography in the los pinos  
729 mountains, sevilleta national wildlife refuge. [https://doi.org/10.6073/pasta/  
730 dd06df3f950afe4a4642306182237d13](https://doi.org/10.6073/pasta/dd06df3f950afe4a4642306182237d13).
- 731 Miller, T. E., Louda, S. M., Rose, K. A., and Eckberg, J. O. (2009). Impacts of insect  
732 herbivory on cactus population dynamics: experimental demography across an envi-  
733 ronmental gradient. *Ecological Monographs*, 79(1):155–172.
- 734 Miller, T. E., Williams, J. L., Jongejans, E., Brys, R., and Jacquemyn, H. (2012). Evolution-  
735 ary demography of iteroparous plants: incorporating non-lethal costs of reproduction  
736 into integral projection models. *Proceedings of the Royal Society B: Biological Sciences*,  
737 279(1739):2831–2840.

- 738 Ochocki, B. M., Drees, T., and Miller, T. E. (2023). Density-dependent demography of  
739 creosote bush (*larrea tridentata*) along grass-shrub ecotones. <https://doi.org/10.6073/pasta/ca53c16f16dcf9fb11f3ee99ea5445ac>.
- 740
- 741 Ohm, J. R. and Miller, T. E. (2014). Balancing anti-herbivore benefits and anti-pollinator  
742 costs of defensive mutualists. *Ecology*, 95(10):2924–2935.
- 743 Ozgul, A., Childs, D. Z., Oli, M. K., Armitage, K. B., Blumstein, D. T., Olson, L. E., Tul-  
744 japurkar, S., and Coulson, T. (2010). Coupled dynamics of body mass and population  
745 growth in response to environmental change. *Nature*, 466(7305):482–485.
- 746 Peterson, M. L., Morris, W., Linares, C., and Doak, D. (2019). Improving structured  
747 population models with more realistic representations of non-normal growth. *Methods  
748 in Ecology and Evolution*, 10(9):1431–1444.
- 749 Plard, F., Schindler, S., Arlettaz, R., and Schaub, M. (2018). Sex-specific heterogene-  
750 ity in fixed morphological traits influences individual fitness in a monogamous bird  
751 population. *The American Naturalist*, 191(1):106–119.
- 752 Rees, M., Childs, D. Z., and Ellner, S. P. (2014). Building integral projection models: a  
753 user's guide. *Journal of Animal Ecology*, 83(3):528–545.
- 754 Rees, M. and Ellner, S. P. (2016). Evolving integral projection models: evolutionary  
755 demography meets eco-evolutionary dynamics. *Methods in Ecology and Evolution*,  
756 7(2):157–170.
- 757 Rigby, R. A., Stasinopoulos, M. D., Heller, G. Z., and De Bastiani, F. (2019). *Distributions  
758 for modeling location, scale, and shape: Using GAMLS in R*. CRC press.
- 759 Salguero-Gómez, R. and Casper, B. B. (2010). Keeping plant shrinkage in the demo-  
760 graphic loop. *Journal of Ecology*, 98(2):312–323.
- 761 Schielzeth, H., Dingemanse, N. J., Nakagawa, S., Westneat, D. F., Allegue, H., Teplitsky,  
762 C., Réale, D., Dochtermann, N. A., Garamszegi, L. Z., and Araya-Ajoy, Y. G. (2020).  
763 Robustness of linear mixed-effects models to violations of distributional assumptions.  
764 *Methods in ecology and evolution*, 11(9):1141–1152.
- 765 Schultz, E. L., Eckberg, J. O., Berg, S. S., Louda, S. M., and Miller, T. E. (2017). Native  
766 insect herbivory overwhelms context dependence to limit complex invasion dynamics  
767 of exotic weeds. *Ecology letters*, 20(11):1374–1384.

- 768 Shriner, R. K., Cutler, K., and Doak, D. F. (2012). Comparative demography of an epi-  
769 phytic lichen: support for general life history patterns and solutions to common prob-  
770 lems in demographic parameter estimation. *Oecologia*, 170:137–146.
- 771 Stasinopoulos, D. M., Rigby, R. A., et al. (2007). Generalized additive models for location  
772 scale and shape (gamlss) in r. *Journal of Statistical Software*, 23(7):1–46.
- 773 Stubberud, M. W., Vindenes, Y., Vøllestad, L. A., Winfield, I. J., Stenseth, N. C., and Lan-  
774 gangen, Ø. (2019). Effects of size-and sex-selective harvesting: An integral projection  
775 model approach. *Ecology and Evolution*, 9(22):12556–12570.
- 776 Wan, X., Wang, W., Liu, J., and Tong, T. (2014). Estimating the sample mean and stan-  
777 dard deviation from the sample size, median, range and/or interquartile range. *BMC*  
778 *medical research methodology*, 14:1–13.
- 779 Wilber, M. Q., Langwig, K. E., Kilpatrick, A. M., McCallum, H. I., and Briggs, C. J. (2016).  
780 Integral projection models for host–parasite systems with an application to amphibian  
781 chytrid fungus. *Methods in Ecology and Evolution*, 7(10):1182–1194.
- 782 Williams, J. L., Miller, T. E., and Ellner, S. P. (2012). Avoiding unintentional eviction from  
783 integral projection models. *Ecology*, 93(9):2008–2014.
- 784 Wood, S. (2017). *Generalized Additive Models: An Introduction with R*. Chapman and  
785 Hall/CRC, 2 edition.
- 786 Zhang, J. L. (2014). Comparative investigation of three bayesian p values. *Computational*  
787 *Statistics & Data Analysis*, 79:277–291.

# Appendices

## 788 S.1 The Jones-Pewsey distribution

789 Jones and Pewsey (2009) introduced a simple, tractable generalization of the Normal dis-  
790 tribution with two additional parameters determining asymmetry (skewness), and tail  
791 weight (kurtosis) which can be either lighter or heavier than the Gaussian. It is defined  
792 as a transformation of a Normal(0,1) random variable using the hyperbolic sine func-  
793 tion ( $\sinh$ ) and its inverse ( $\text{asinh}$ ), as follows. The distribution family's base probability  
794 density  $f_{\epsilon,\delta}$  is the probability density of the random variable  $X_{\epsilon,\delta}$  where

795 
$$Z = \sinh(\delta \text{ asinh}(X_{\epsilon,\delta}) - \epsilon) \quad (\text{S.1})$$

796 and  $Z$  has a Normal(0,1) distribution. Equivalently,

797 
$$X_{\epsilon,\delta} = \sinh\left(\frac{1}{\delta} \text{ asinh}(Z) + \frac{\epsilon}{\delta}\right). \quad (\text{S.2})$$

798 Parameters  $\delta = 1, \epsilon = 0$  give the Normal(0,1) distribution. Skewness has the sign of  $\epsilon$ ,  
799 and  $\delta > 0$  controls tail weight, with heavier than Gaussian tails for  $\delta < 1$  and lighter  
800 than Gaussian tails for  $\delta > 1$ . A formula for the density  $f_{\epsilon,\delta}$  is given by Jones and Pewsey  
801 (2009, eqn. 2). The general four-parameter family with location parameter  $\mu$  and scale  
802 parameter  $\sigma$  is defined as the probability densities of  $\mu + \sigma X_{\epsilon,\delta}$ . We refer to this as the  
803 JP distribution family.

804 As is unfortunately the case for most four-parameter distributions  $\mu$  is not the mean,  
805  $\sigma$  is not the standard deviation,  $\epsilon$  is not the skew and  $\delta$  is not the kurtosis. All else being  
806 equal, larger  $\mu$  gives a larger mean, larger  $\sigma$  gives a higher standard deviation, higher  
807  $\epsilon$  gives higher asymmetry, and higher  $\delta$  gives heavier tail weight. But each moment is  
808 jointly determined by all four parameters.

809 The main advantage of the JP distribution is that the attainable combinations of  
810 skewness and kurtosis are very broad, compared to other four-parameter families, and  
811 come very close to the theoretical limits on kurtosis as a function of skewness (Jones and  
812 Pewsey, 2009, Fig. 2). Additionally, being a transformation of the Normal makes it very  
813 simple to generate random numbers from the distribution, and to compute probability  
814 density, cumulative distribution, and quantile functions. There are also simple analytic  
815 formulas for the first four moments (Jones and Pewsey, 2009, p. 764) which we use below  
816 to define a centered and scaled version in which  $\mu$  and  $\sigma$  are the mean and standard  
817 deviation.

818 The definition (S.2) shows that the distribution depends on  $\epsilon$  only through the ratio  
 819  $\epsilon/\delta$ . We have found that this property can be problematic for estimating distribution  
 820 parameters. Even with good sized ( $n = 250$  or  $500$ ) data sets generated from the distri-  
 821 bution with known parameters, both maximum likelihood and Bayesian estimation were  
 822 unstable for some values of  $\epsilon$  and  $\delta$ , occasionally yielding estimates far from the truth.  
 823 One cause was a ridge in the  $(\epsilon, \delta)$  likelihood surface with a constant of  $\epsilon/\delta$ . Another is  
 824 that when  $\delta$  is large, changes in  $\epsilon$  have little effect.

825 To avoid that problems, we reparameterize the distribution as follows:

$$826 \quad X_{\lambda, \tau} = \sinh(e^{-\tau} \operatorname{asinh}(Z) + \lambda). \quad (\text{S.3})$$

827 Thus, the two parameterizations are related by

$$828 \quad \delta = e^\tau, \epsilon = \delta\lambda = e^\tau\lambda. \quad (\text{S.4})$$

829 The definition of  $\tau$  allows it to take any real value, with negative values giving thinner  
 830 than Gaussian tails and positive values giving fatter than Gaussian tails.  $\lambda$  also can take  
 831 any real value, and the distribution's skew has the same sign as  $\lambda$ . Because the sinh  
 832 function is nonlinear, it is still the case that the skew depends on  $\tau$  as well as  $\lambda$ , but the  
 833 "crosstalk" between the kurtosis and skew parameters is weaker. As a result, we found  
 834 that maximum likelihood estimation of parameter values was generally more reliable if  
 835 the distribution is parameterized in terms of  $\tau$  and  $\lambda$ .

## 836 S.2 Estimating mixed-effects models using shrinkage

837 Ecologists often fit demographic and other statistical models that include random effects  
 838 terms to quantify variation among years, spatial locations, individuals, etc. Random  
 839 effects are a natural choice when interest centers on the magnitude of variation (e.g., how  
 840 much does mortality vary among years?) rather than individual values (e.g., mortality  
 841 in 2013). They also allow each estimate to "borrows strength" from others, so that (for  
 842 example) the estimate from a year with small sample size (and thus large sampling  
 843 variability) is shifted towards the center of the overall distribution.

844 Specialized software is often used to fit such models, such as the **nlme**, **lme4**, **mgcv**  
 845 and **gamm4** libraries in R, but these only allow a small subset of the distribution families  
 846 we want to consider for modeling growth increments (the **gamLss** package allows many  
 847 distribution families, but in our experience, even when random effects are simple in  
 848 structure the fitting algorithms often fail to converge or fail to find the global optimum).

849 One way past this limitation is Bayesian estimation, using STAN with user-written  
850 (or borrowed) code for the chosen growth distribution (see section XX for an example).  
851 In this appendix we describe another option, introduced by Link and Nichols (1994)  
852 and Gould and Nichols (1998): fitting a fixed-effects model by Maximum Likelihood,  
853 followed by shrinkage of coefficient estimates. None of the ideas here are original. The  
854 material overlaps Appendix S1 of Metcalf et al. (2015), but for completeness we make  
855 it self-contained. Appendix D of Cooch and White (2020) (written by K.D. Burnham)  
856 provides more details and examples in the context of capture-recapture analysis.

857 Here we explain shrinkage using a simple model based on our analysis of *Pseu-*  
858 *doroegneria spicata*. That model includes random effects for between-year variation in  
859 the slope and intercept of future size (log area) as a function of initial size. To keep  
860 the example simple, we assume that initial size and year are the only covariates, and  
861 we assume that growth increments follow a skew-Normal distribution with noncon-  
862 stant variance and constant skew parameter. Code for this example is in the script  
863 `SimpleShrinkageExample.R`. The first part of the script generates an artificial data set  
864 by fitting the model to a subset of the growth data (20th century Control plots), and  
865 randomly generating new “size next year” values for each individual in the actual data  
866 set. The second part contains the “data” analysis.

867 As in our *P. spicata* analysis, we assumed that that the skew and kurtosis parameters  
868 were functions of the location parameter; this dominated ( $\Delta AIC \approx 30$ ) the alternate  
869 model with skew and kurtosis depending on initial size. The analogous Gaussian model,  
870 with constant variance, could be fitted as follows using `lmer`:

871 `lmer(new.size ~ init.size + (init.size|year), data=growthData, REML=TRUE);`  
872 where `growthData` is a data frame holding the data with year as an unordered factor.  
873 For our skew-Normal model, we instead use maximum likelihood with all between-year  
874 variation included as fixed effects. The appropriate design matrix is easily constructed  
875 using the `model.matrix` function:

876 `U = model.matrix(~ year + init.size:year - 1, data=growthData)`

877 If there are  $T$  years, the matrix `U` specified in this way has  $2T$  columns corresponding to  
878  $n$  annual intercepts and  $T$  annual slopes.

879 Using this design matrix, we can readily write a log likelihood function for use with  
880 the `maxLik` package, with a log link function for the variance because it is necessarily  
881 positive:

882 `LogLik=function(pars,new.size,U){`

```

883 pars1 = pars[1:ncol(U)]; pars2=pars[-(1:ncol(U))];
884 mu = U%*%pars1;
885 sigma = exp(pars2[1]+pars2[2]*mu);
886 dSN1(new.size, mu=mu, sigma=sigma, nu=pars2[3], log=TRUE)
887 }

```

888 Parameters and their standard errors can then be estimated with `maxLik`, starting  
889 from a random guess:

```

890 start=c(runif(ncol(U)), rep(0,3))
891 out=maxLik(logLik=LogLik,start=start, new.size=simData$new.size,U=U,
892 method="BHHH",control=list(iterlim=5000,printLevel=1),finalHessian=TRUE);
893 coefs = out$estimate; # parameters
894 V = vcov(out); SEs = sqrt(diag(V)); # standard errors

```

895 In real life we would repeat the optimization several times with several different starting  
896 values, to be confident that the optimal parameter values had been found.

897 Focus now on the year-specific intercept parameters  $\hat{a}_t, t = 1, 2, \dots, T$ . We can view  
898 the year-specific estimates  $\hat{a}_t$  as consisting of unobserved true values  $a_t$  plus sampling  
899 error:

$$900 \quad \hat{a}_t = a_t + \varepsilon_t \quad (S.5)$$

901 Because of the sampling errors, the sample variance of the estimates  $\hat{a}_t$  is an upward-  
902 biased estimate of the true across-year variance in the parameter. That is undesirable if  
903 the model will be used to project how temporal variability affects population dynamics.  
904 However, maximum likelihood estimation gives us an approximate variance-covariance  
905 matrix  $\hat{V}$  of the sampling errors,  $V$  in the code above. With that information, we can  
906 estimate the parameters of a random effects model for the intercept parameters, and  
907 thereby improve the year-specific estimates and the estimate of the across-year variance.

908 The model is as follows. We make the standard mixed-models assumptions that the  
909  $a_t$  are drawn independently from some fixed distribution with unknown variance  $\sigma^2$ .  
910 We also assume that the estimates  $\hat{a}_t$  are unbiased, that is

$$911 \quad \mathbb{E}(\varepsilon_t | a_t) = 0. \quad (S.6)$$

912 These are optimistic assumptions, but not excessively optimistic. Some degree of tem-  
913 poral correlation will often be present, and as we explain at the end, it is theoretically  
914 possible to account for it. Maximum likelihood parameter estimates are not unbiased,  
915 but if the assumptions of maximum likelihood are satisfied the bias is asymptotically

916 negligible compared to the standard error (the bias scales as the inverse of sample size,  
 917 the standard error as the square root of the inverse of sample size).

918 Let  $S^2$  denote the sample variance of the estimates  $\hat{a}_t$ . It can then be shown that

$$919 \quad \mathbb{E}(S^2) = \sigma^2 + \frac{1}{T} \sum_{t=1}^T \mathbb{E}Var(\varepsilon_t) - \frac{1}{T(T-1)} \sum_{i=1}^{j-1} \sum_{j=1}^T \mathbb{E}Cov(\varepsilon_i, \varepsilon_j). \quad (\text{S.7})$$

920 This is eqn. (1) in Gould and Nichols (1998) in our notation, without the term that results  
 921 from temporal autocorrelation.

922 The terms besides  $\sigma^2$  on the right-hand are the expected impact of sampling error  
 923 on the across-year variance of the parameter estimates; their presence makes  $S^2$  a biased  
 924 estimated of  $\sigma^2$ . However, all of those terms correspond to entries in the variance-  
 925 covariance matrix  $V$ . We can therefore use our estimated variance-covariance matrix  $\hat{V}$   
 926 to removes the bias due to sampling variability:

$$927 \quad \hat{\sigma}^2 = S^2 - \frac{1}{T} \sum_{t=1}^T \hat{V}_{t,t} + \frac{1}{T(T-1)} \sum_{i=1}^{j-1} \sum_{j=1}^T \hat{V}_{i,j}. \quad (\text{S.8})$$

928  $\hat{\sigma}^2$  estimates the variance of the distribution from which the  $a_t$  are assumed to be drawn.

929 Using that estimate, we can adjust the year-specific estimates to reduce the ex-  
 930 pected impact of sampling error. Depending on your purposes, there are two possible  
 931 adjustments. The first option is the one used in the popular capture-recapture analysis  
 932 software Mark Cooch and White (2020),

$$933 \quad \tilde{a}_t = \bar{a}_t + \sqrt{\frac{\hat{\sigma}^2}{\hat{\sigma}^2 + \hat{V}_{t,t}}} (\hat{a}_t - \bar{a}_t). \quad (\text{S.9})$$

934 The name “shrinkage” comes from the fact that each estimate is adjusted towards the  
 935 overall mean, with larger adjustments of values that have higher estimated sampling  
 936 error variance,  $\hat{V}_{t,t}$ . This shrinkage estimate has the property that the expected sample  
 937 variance of the adjusted estimates  $\tilde{a}_t$  is very close to  $\hat{\sigma}^2$ , so the  $\tilde{a}_t$  approximate the actual  
 938 amount of parameter variation.

939 The second is to replace  $\hat{a}_t$  by the least-squares estimate of  $a_t$  under the additional  
 940 assumption that the  $a_t$  are drawn from a Gaussian distribution; this is given by

$$941 \quad \tilde{a}_t = \bar{a}_t + \frac{\hat{\sigma}^2}{\hat{\sigma}^2 + \hat{V}_{t,t}} (\hat{a}_t - \bar{a}_t). \quad (\text{S.10})$$

942 This option is theoretically preferable if the Gaussian assumption is reasonable, and you  
 943 are more interested in year-specific values rather than across-year variance. However,  
 944 Metcalf et al. (2015) found that even (S.9), which does less shrinkage, resulted in a small  
 945 downward bias in the temporal variance of population growth rates. This argues for  
 946 always using the first option, and we do the same here.

947 We differ from MARK, however, in using (S.8) rather than an iterative method  
 948 that takes (S.8) as its starting estimate and refines the estimate by using weighted least  
 949 squares based on the current estimate. Metcalf et al. (2015) found, in simulation studies,  
 950 that the iterative method was either slightly beneficial or wildly inaccurate. We therefore  
 951 advise against it.

952 Finally, as mentioned above, the estimate of  $\sigma^2$  can account for temporal autocor-  
 953 relation in the  $a_t$ . When present, those correlations add a term to eqn. (S.7) (see eqn.  
 954 (1) in Gould and Nichols (1998)), which can be estimated from the sample autocorre-  
 955 lation of the  $\hat{a}_t$ . We do not recommend doing this (and therefore omit the formulas)  
 956 because the autocorrelations can only be reliably estimated if they fall to nearly zero  
 957 within lag  $m \ll T$ , in which case the autocorrelation term is small (specifically,  $O(m/T)$ ).  
 958 Otherwise, the random error from using poorly estimated autocorrelations is likely to  
 959 outweigh the small bias from omitting that term.

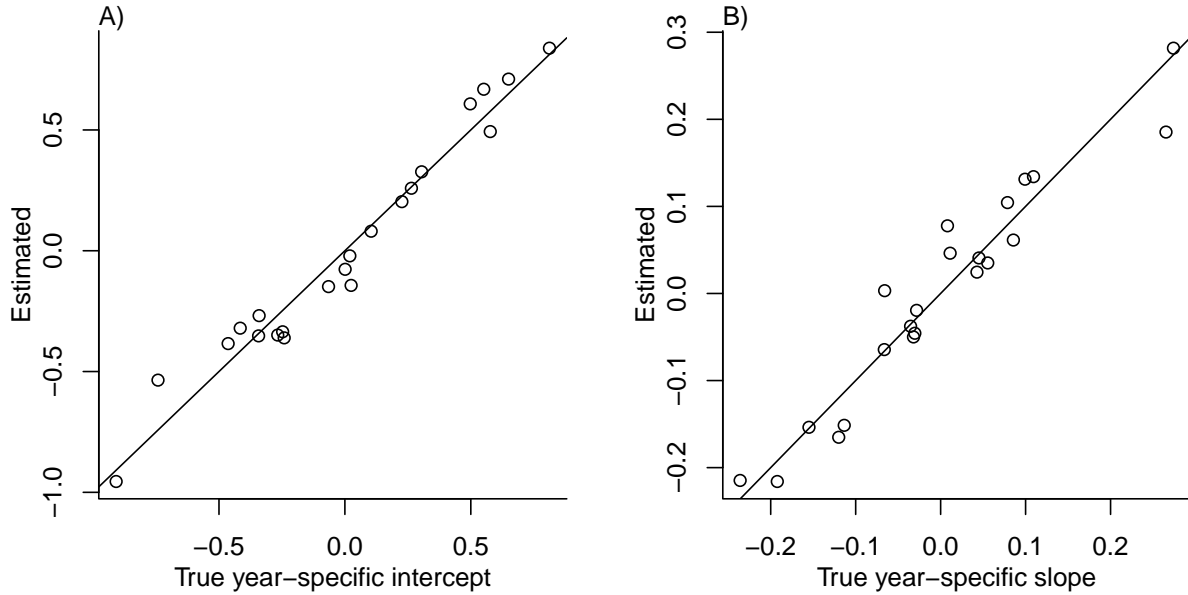
960 The take-home message is that estimating random effects from the regression coef-  
 961 ficients is very simple:

```

962 # Variance-covariance matrices for intercepts and slopes
963 V1 = V[1:T,1:T]; V2 = V[(T+1):(2*T),(T+1):(2*T)];
964 # Extract year-specific intercepts, center them to zero
965 fixed.fx = coefs[1:T]; fixed.fx = fixed.fx-mean(fixed.fx);
966
967 # Estimate sigma^2
968 var.hat = mean(fixed.fx^2) - mean(diag(V1)) +
969             (sum(V1)-sum(diag(V1)))/(2*T*(T-1));
970
971 # Shrink deviations from the mean
972 shrinkRanIntercept = fixed.fx*sqrt(var.hat/(var.hat + diag(V1)));
973
974 # Do it all again for the slopes
975 fixed.fx2 = coefs[(T+1):(2*T)]; fixed.fx2 = fixed.fx2-mean(fixed.fx2);
976 var2.hat = mean(fixed.fx2^2) - mean(diag(V2)) +
977             (sum(V2)-sum(diag(V2)))/(2*T*(T-1));
  
```

```
978 shrinkRanSlope = fixed.fx2*sqrt(var2.hat/(var2.hat + diag(V2)));
```

979 The figure below shows the results for one artificial PSSP “data” set, having  $T = 22$   
980 years and growth measurements on about 175 individuals/year on average. The true  
981 random year effects (the ones used to generate the data) are recovered with good accu-  
982 racy and no bias. In particular there is no sign of extreme values being pulled in too  
983 far towards the mean, which would cause an S-shaped graph of estimated versus true  
984 values.



### 985 S.3 Additional case studies

#### 986 S.3.1 Case study: Sea fan corals, *Gorgonia ventalina*

987 Bruno et al. (2011) developed an IPM to understand the rise and fall of a fungal pathogen  
988 *Aspergillus sydowii* in Caribbean sea fan corals *G. ventalina*. The model was based on re-  
989 peated observations of marked corals in permanent transects at several sites near Aku-  
990 mal, Mexico, recording disease status (infected/uninfected) and the area of uninfected  
991 tissue. The epidemic peak had passed and disease incidence was already low, so in-  
992 fected fans were relatively infrequent. We therefore limit the analysis here to uninfected  
993 individuals. Bruno et al. (2011) found statistically significant year and site effects, but  
994 as those explained a very small fraction of the variation in growth increments, they  
995 fitted a single growth model to data pooled across years and sites. We do the same  
996 here. The pooled data set consists of 358 observed size transitions. The data exhibited

997 size-dependent variance in growth (change in area,  $cm^2$ ). Bruno et al. (2011) chose to sta-  
998 bilize the variance by cube-root transforming size, and then fitting the standard model  
999 with Gaussian growth increments. Here we take a different approach, using natural log  
1000 transformation of area and modeling size-dependent variance.

1001 With initial size as the only predictor, a simple way to fit a Gaussian model with  
1002 nonconstant variance is the `gam` function in `mgcv` library (Wood, 2017) using the `gaulss`  
1003 family. The mean and standard deviation are both fitted as smoothing spline functions  
1004 of initial size, and the `predict` function returns the fitted mean and also the inverse of  
1005 the fitted standard deviations with which we can compute the scaled residuals:

```
1006 # XH is a data frame holding the data
1007 # logarea.t0, .t1 denote initial and final values of log-transformed area
1008 fitGAU <- gam(list(logarea.t1~ s(logarea.t0), ~ s(logarea.t0)),
1009   data=XH, gamma=1.4, family=gaulss())
1010 fitted_all = predict(fitGAU,type="response");
1011 fitted_sd = 1/fitted_all[,2];
1012 scaledResids = residuals(fitGAU,type='response')/fitted_sd;
```

1013 Fig. S-1A shows the log-transformed data and Gaussian model. The mean function  
1014 (solid red curve) is visually nearly linear, but the fitted spline is strongly favored over a  
1015 linear model for the mean ( $\Delta AIC \approx 9$ ). The spline for standard deviation  $\sigma$  versus initial  
1016 size reflects the evident greater variability in growth at smaller sizes.

1017 There are no blatant signs of trouble in the pilot Gaussian model, but quantile re-  
1018 gressions on the scaled residuals, and the NP Skewness and Kurtosis metrics derived  
1019 from them (Eq. 3 and 4), suggest deviations from normality (Fig. S-1B). Specifically,  
1020 skewness switches from negative to positive across the size range, with smaller corals  
1021 more prone to extreme shrinkage and larger corals more prone to extreme growth. Kur-  
1022 tosis also changes direction over the size distribution, with thinner tails than Gaussian  
1023 at small sizes and fatter tails at large sizes. The fitted nonparametric moments suggest  
1024 that the upper and lower tails of size transition probabilities may differ by up to 20%,  
1025 and the weight of the tails may be 20% greater or less than Gaussian, depending on  
1026 initial size – not overwhelming deficiencies, but not trivial either. Are these deviations  
1027 from normality severe enough to warrant a second, non-Gaussian iteration of growth  
1028 modeling? To answer that question, we simulated data from the fitted Gaussian model  
1029 and examined whether key properties of the simulated data are consistent with those  
1030 of the real data – this is the ultimate litmus test for a growth model's adequacy and  
1031 should be a standard element of IPM construction, in our opinion. If the simulated data

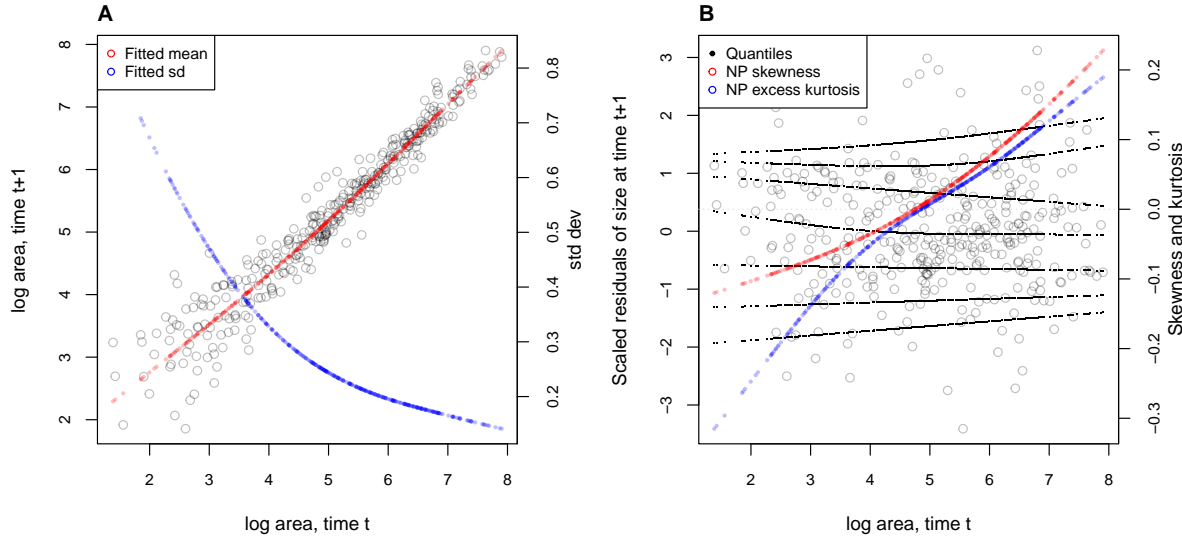


**Figure S-1:** **A**, Size transition data for sea fan corals, *Gorgonia ventalina*, and fitted gam with mean (red) and standard deviation (blue) of future size conditional on current size. **B**, Quantile regressions of scaled residuals on size and nonparametric estimates of skewness (red) and excess kurtosis (blue) derived from them. Black lines in **B** show the 5th, 10th, 25th, 50th, 75th, 90th, and 95th quantiles. Figure made by script AkumalCorals\_qgam.R.

1032 are not consistent with the real data, it is time to choose a better distribution (Fig. 1).  
 1033 In this case, most of 100 Gaussian model simulations are out of line with the skew at  
 1034 smallest and largest sizes, and excess kurtosis observed at moderately large sizes (Fig.  
 1035 S-2 CD). For at least some parts of the size distribution, a non-Gaussian model would  
 1036 better capture size transitions.

1037 We sought a distribution that could accommodate the observed changes in the sign  
 1038 of skewness and excess kurtosis. We chose the sinh-arcsinh (SHASH) distribution, a  
 1039 four-parameter distribution that, conveniently, is included in **mgcv**'s **gam()** function.  
 1040 For consistency with the Gaussian for location and scale, specification of basis functions  
 1041 ( $k = 4$ ) is limited to parameters for skewness and kurtosis:

```
1042 fitSHASH <- gam(list(logarea.t1 ~ s(logarea.t0), # <- location
1043 ~ s(logarea.t0), # <- log-scale
1044 ~ s(logarea.t0,k=4), # <- skewness
1045 ~ s(logarea.t0,k=4)), # <- log-kurtosis
1046 data = XH, gamma = 1.4, family = shash, optimizer = "efs")
```

1047 The fitted model's mean and variance are nearly identical to the Gaussian (Fig. S-2AB),  
 1048 and the fitted trends in skewness and kurtosis are much less "wiggly" than the estimate

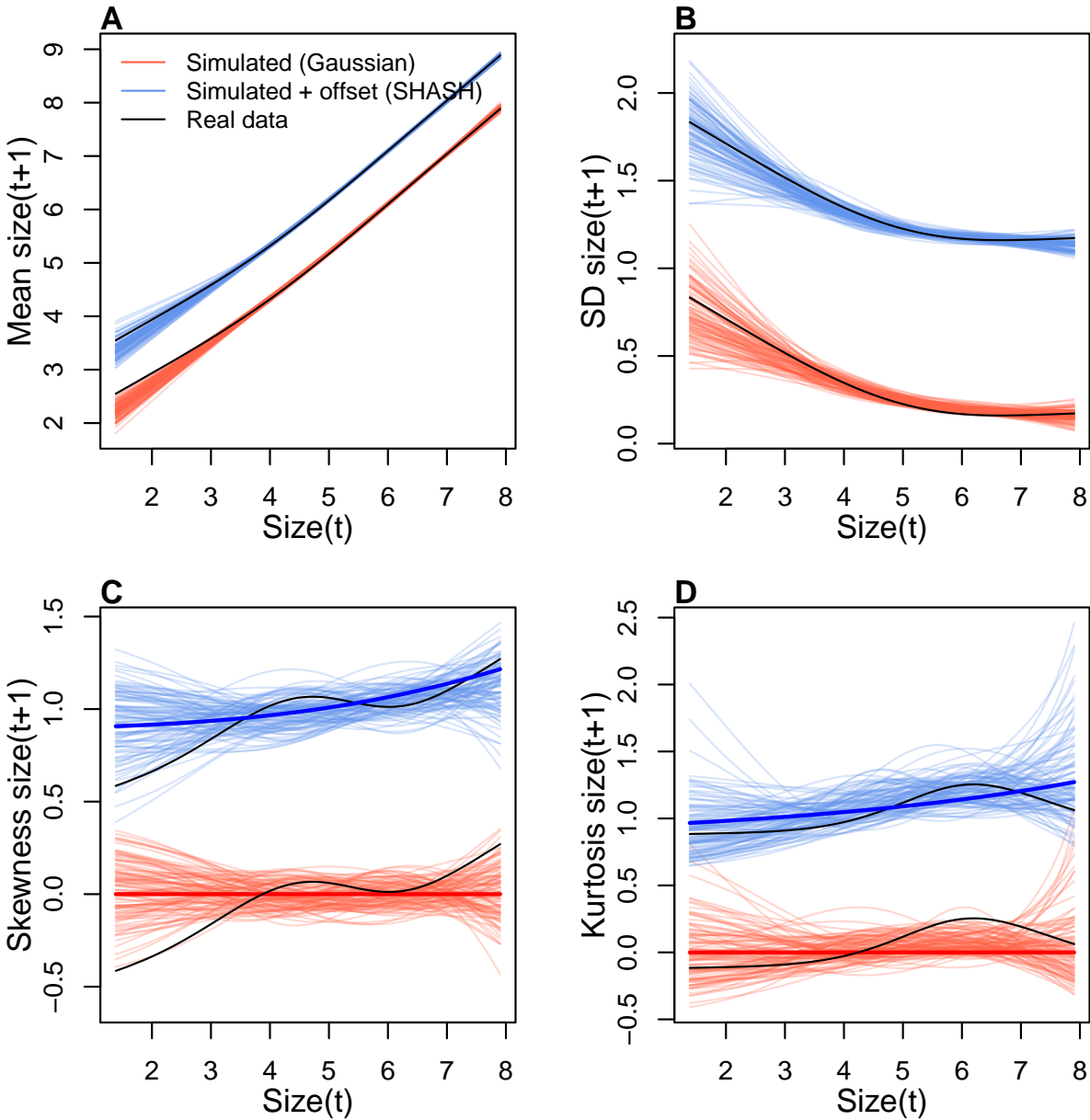


**Figure S-2:** Comparisons among real coral data and data simulated from Gaussian and SHASH growth models for mean, standard deviation, NP skewness, and NP excess kurtosis of future size conditional on current size. Note that plotted values for the SHASH are offset by one unit to allow comparisons. In the skewness and kurtosis panels, the darker solid curves show the values for the fitted growth models. Figure made by script AkumalCorals\_qgam.R.

from the data (Fig. S-2CD). Nonetheless, data simulated from the SHASH model are more consistent with the real data, with more SHASH data sets matching or exceeding the largest skewness and kurtosis values observed (Fig. S-2CD). If one cares to quantify

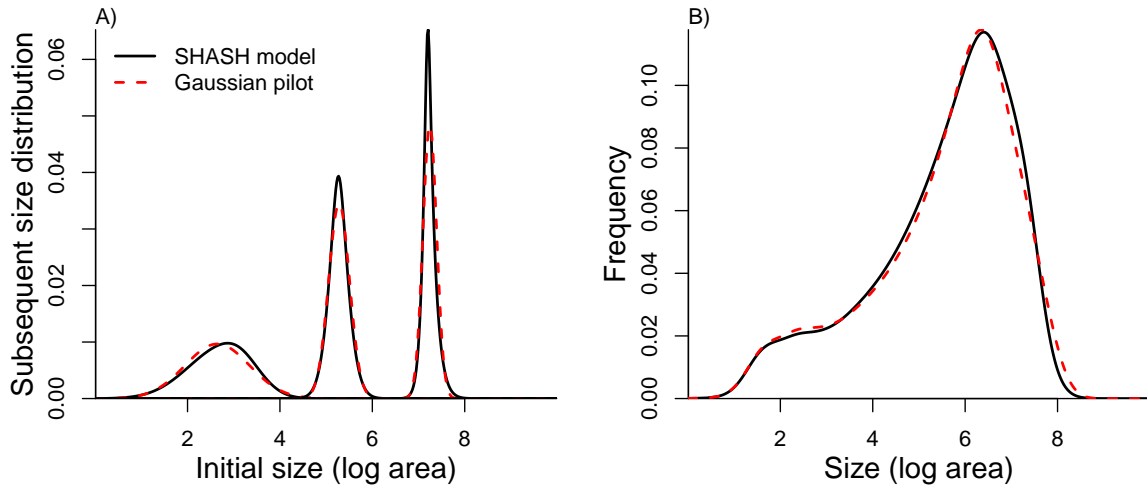


**Figure S-3:** Comparisons between the fitted SHASH growth model (solid black curves) and the Gaussian pilot model (dashed red curves) for sea fans *G. ventalina*. A) Predicted frequency distributions of size in year  $t + 1$  for three different values of size in year  $t$ . The leftmost pair of curves are for initial size equal to the median size of a new recruit (data from (Bruno et al., 2011)); central pair is for the median initial size of uninfected individuals; rightmost pair are for the 95th percentile initial size for uninfected individuals. B) Steady-state size distributions resulting from a constant unit input of new recruits. As in Bruno et al. (2011) we assume that larvae are very widely dispersed, so that the number of recruits arriving at any one location is independent of the local population abundance or structure. Size distribution of recruits was described by a kernel density estimate based on the measured sizes of known new recruits ( $n = 9$ ). Figure made by script AkumalCoralsIPMs.R.

the difference between models, the SHASH model is clearly favored by AIC ( $\Delta AIC = 5.45$ ) despite having twice as many parameters to fit.

What, then, have we gained by fitting a better growth model? Fig. S-3A compares the predicted distributions of subsequent size in the fitted model and Gaussian pilot models, for the median size of a new recruit (leftmost pair of curves), the median initial size (central curves), and the 95th percentile of initial size in the data (rightmost curves). The differences are small, and most pronounced for the smallest size, where recruits are predicted to grow slightly larger under the SHASH model than the Gaussian model. The direction of this difference was surprising, because the SHASH has negative skew at small sizes in the data. However, the SHASH model also gives a better prediction of mean growth at small sizes than the Gaussian model. At intermediate sizes the predictions are nearly identical; at large sizes the SHASH has slightly lower standard deviation, but fatter tails (excess kurtosis). Fig. S-3B shows the predicted steady-state size distributions resulting from a constant unit input of recruits. Again, the differences

1066 are very subtle. Finally, the Gaussian and SHASH growth models predict very similar  
1067 mean life span (17.7 and 17.9 years, respectively).

1068 From these outputs, there is little evidence that improved modeling of coral growth  
1069 meaningfully improved biological inferences from the IPM. One could argue that it was  
1070 not worth the trouble, even though it was almost no trouble at all. But before fitting  
1071 the SHASH model, we could not have known whether or not it would have made a  
1072 difference.

1073 In this case study we used `gam` to fit both the Gaussian and SHASH models because  
1074 that obviated model selection on functions for mean, variance, and higher moments.  
1075 However, `gam` should be used with caution. Nonparametric regression models notori-  
1076 ously “wag their tails” because the ends of the fitted curve can be pulled close to the  
1077 outermost data points. This is especially problematic for growth modeling, because data  
1078 are typically sparse near the bounds of the size distribution. To minimize the risk of  
1079 overfitting we specified the number of “knots” (`k=4`) and used `gamma=1.4` to overweight  
1080 model degrees of freedom as suggested by Gu (2013, sec. 3.2). But it is always impor-  
1081 tant to plot the fitted splines and make sure they do not wag unrealistically. If they do,  
1082 parametric regression may be a better choice.

### 1083 S.3.2 Case study: creosotebush, *Larrea tridentata*

1084 Our next case study comes from our studies of the woody shrub creosotebush (*Larrea tri-*  
1085 *dentata*) at the Sevilleta Long-Term Ecological Research (LTER) site in central New Mex-  
1086 ico, US. At this site as elsewhere in the Southwest US, creosotebush is encroaching into  
1087 desert grassland habitats. The data described here were collected along transects span-  
1088 ning grass-shrub ecotones to understand patterns of density dependence in creosotebush  
1089 demography. Specifically, we asked whether fitness is maximized approaching zero den-  
1090 sity at the leading edge of the expansion front (consistent with ‘pulled’ expansion), or  
1091 whether there is a demographic advantage for shrubs at higher density due to positive  
1092 feedbacks expected for ecosystem engineers (leading to ‘pushed’ expansion). Our pub-  
1093 lished study (Drees et al., 2023) used a spatial integral projection model (SIPM) to predict  
1094 the speed of shrub encroachment, assuming normally-distributed size transitions. Here  
1095 we step through our suggested workflow to ask whether a non-Gaussian model would  
1096 have been more faithful to the data, and how such an improvement would influence  
1097 predictions for the speed of encroachment.

1098 Growth data come from 522 shrubs censused longitudinally over four years (2013-  
1099 2017). Census individuals occurred along 12 replicate transects (200 to 600 m in length)

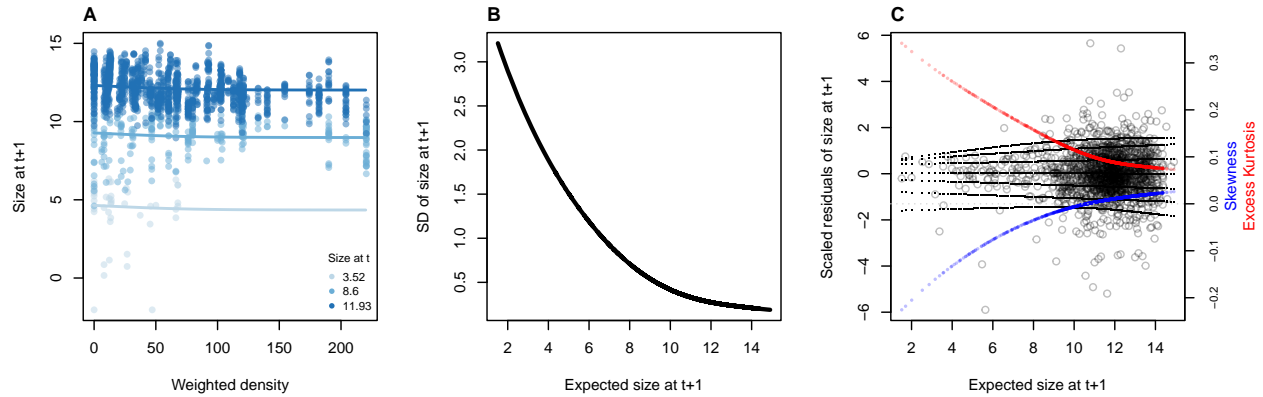


**Figure S-4:** **A**, Creosotebush size transition data with respect to initial size (colors) and local weighted density (sum of sizes of all plants within a five-meter transect window). Size is quantified as the natural logarithm of plant volume ( $cm^3$ ). **B**, Standard deviation of size at time  $t + 1$  as a function of expected size at  $t + 1$  (the fitted values), estimated by iterative re-weighting. **C**, Quantile regressions of scaled residuals on size and nonparametric estimates of skewness (blue) and excess kurtosis (red) derived from them. Black lines in **C** show the 5th, 10th, 25th, 50th, 75th, 90th, and 95th quantiles. All figures made by script `creosote_growth_modeling.R`.

1100 that spanned gradients of shrub density along shrub-grass ecotones. Size was measured as volume of an elliptical cone based on height and width measurements; the size  
 1101 variable of the IPM was the natural logarithm of volume ( $cm^3$ ). For each census individual,  
 1102 we recorded the size and density of all conspecifics within the five-meter transect  
 1103 “window” in which it occurred, and took the sum of all sizes within the window as a  
 1104 weighted measure of local density. The data are available in Ochocki et al. (2023).

1105  
 1106 As an initial Gaussian approach, and following the approach of Drees et al. 2023,  
 1107 we first fit a generalized additive model with `mgcv` that included smooth terms for initial  
 1108 size and weighted density (constrained to four basis functions), plus the random effect  
 1109 of transect. We used the `gaulss` family and, as a starting point, fit a constant standard  
 1110 deviation.

```
1111 LATR_GAU <- gam(list(log_volume_t1~ s(log_volume_t,k=4) +
1112 s(dens_scaled,k=4) + s(unique.transect,bs="re"), ~ 1),
1113 family="gaulss", data=LATR_grow, method="ML", gamma=1.4)
```

1114 Using the fitted values from this initial model, we updated the standard deviation to  
 1115 be a smooth function of fitted values, and iterated the fitting until the weights stopped  
 1116 changing, following the same steps as in the orchid case study.

1117 The resulting Gaussian growth model predicts strong initial size-dependence and  
 1118 weak and slightly nonlinear (but monotonic) negative density dependence (Fig. S-4A).

1119 The model accounts for non-constant variance, which indicate greater dispersion for  
1120 smaller values of expected size (Fig. S-4B). Quantiles of the standardized residuals indi-  
1121 cate that skew and excess kurtosis are both greater at smaller sizes (Fig. S-4C). Skewness  
1122 is close to zero for larger plants (the best-sampled size range) but excess kurtosis re-  
1123 mains positive for large plants (ca. 10% heavier tails than Gaussian). As a candidate  
1124 for improvement, we turned to the Johnson's  $S_U$  (JSU) distribution, a four-parameter,  
1125 leptokurtic distribution capable of skew in either direction.

1126 Following our suggested workflow, rather than re-fitting a JSU model from scratch,  
1127 we parameterize a model where the residuals from the Gaussian model are fitted by  
1128 a JSU distribution. This is relatively easy because the **gamlss.dist** package provides a  
1129 parameterization of the JSU in which the location parameter  $\mu$  is the mean and scale  
1130 parameter  $\sigma$  is the standard deviation (Rigby et al., 2019). We fit the "hybrid" model by  
1131 writing a likelihood function that uses the fitted mean and standard deviation functions  
1132 from Gaussian pilot model, and estimates the parameters that control skewness and  
1133 kurtosis as linear functions of predicted future size. The "hybrid" likelihood looks like  
1134 this:

```
1135 JSULogLik=function(pars){  
1136   dJSU(LATR_grow$log_volume_t1,  
1137     mu=LATR_grow$GAU_mean,  
1138     sigma=LATR_grow$GAU_sd,  
1139     nu = pars[1]+pars[2]*LATR_grow$GAU_mean,  
1140     tau = exp(pars[3]+pars[4]*LATR_grow$GAU_mean), log=TRUE)  
1141 }
```

1142 The mean and standard deviation of the JSU are set to those of the best Gaussian  
1143 model and parameters controlling skewness and kurtosis were fit independently, follow-  
1144 ing our approach to the orchid data. The hybrid JSU model performed well, generating  
1145 simulated data that aligned with the real data better than the best Gaussian model, par-  
1146 ticularly in the standard deviation and kurtosis (Fig. S-5). The JSU model has exactly the  
1147 same mean and standard deviation of future size as the Gaussian, but Fig. S-4 uses the  
1148 quantile-based nonparametric mean and standard deviation. The results show that even  
1149 though the JSU was not fitted to match those, it comes closer than the Gaussian model  
1150 as a result of accounting for the skew and kurtosis.

1151 The improvement of the JSU over the Gaussian growth model, while visually sat-  
1152 isfying, had only weak influence on SIPM results. The Gaussian model slightly over-  
1153 estimated the low-density growth rate, but models using either Gaussian or JSU growth

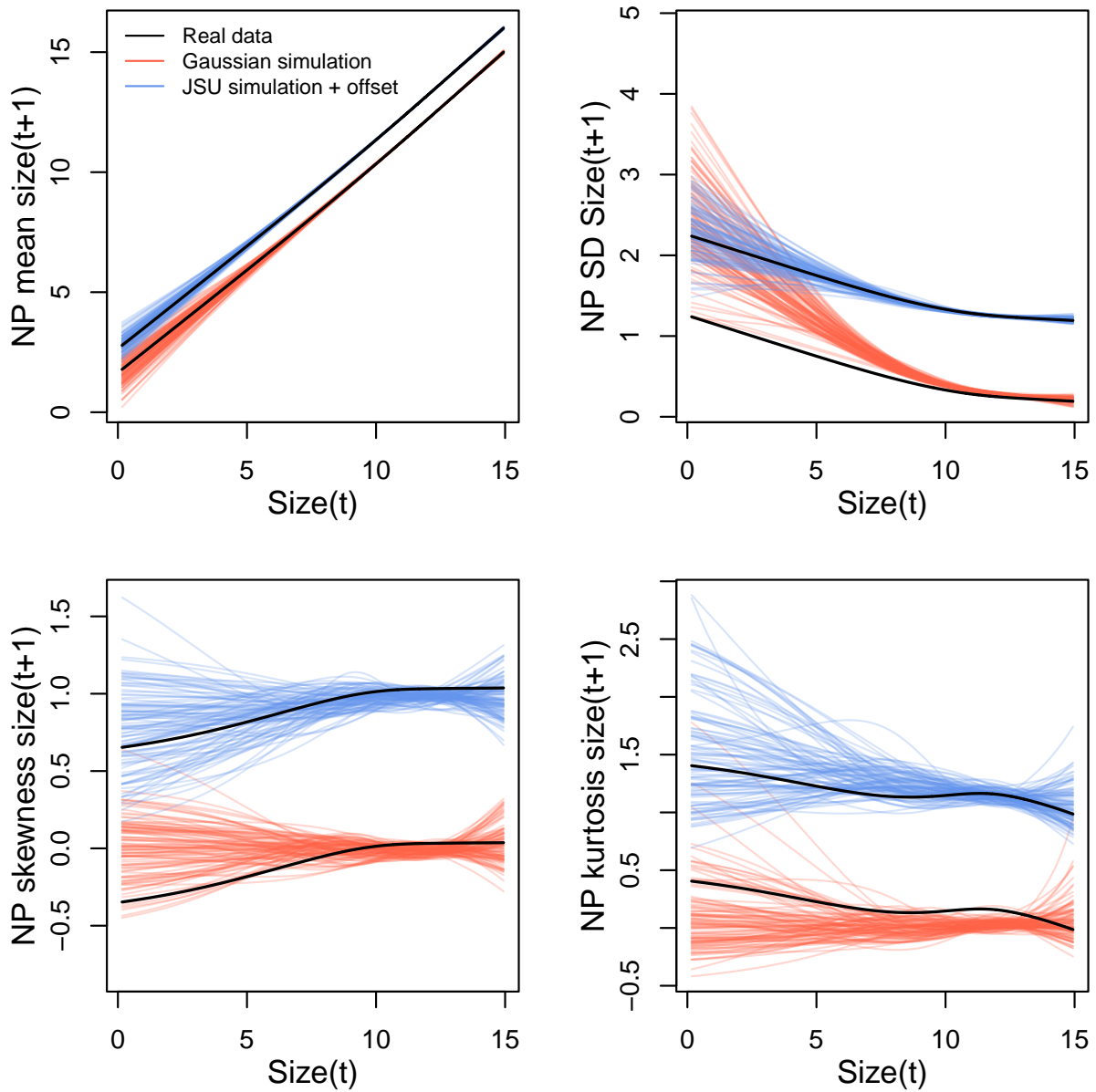


**Figure S-5:** Comparisons between real creosotebush data and data simulated from Gaussian and JSU growth models for nonparametric measures of mean, standard deviation, skewness, and excess kurtosis of future size conditional on current size. Moments of the future size distribution are plotted with respect to initial size; their distribution is also conditional on density but initial size is by far the stronger predictor of future size, so we chose this visualization. Values for the JSU model (and the corresponding “real data” values) are offset vertically by one unit for comparison. Figure made by script `creosote_growth_modeling.R`.

<sup>1154</sup> kernels had very similar monotonic decreases in  $\lambda$  with increasing local density, and  
<sup>1155</sup> nearly identical wave velocities (Fig. S-6). This species has very low mortality risk once

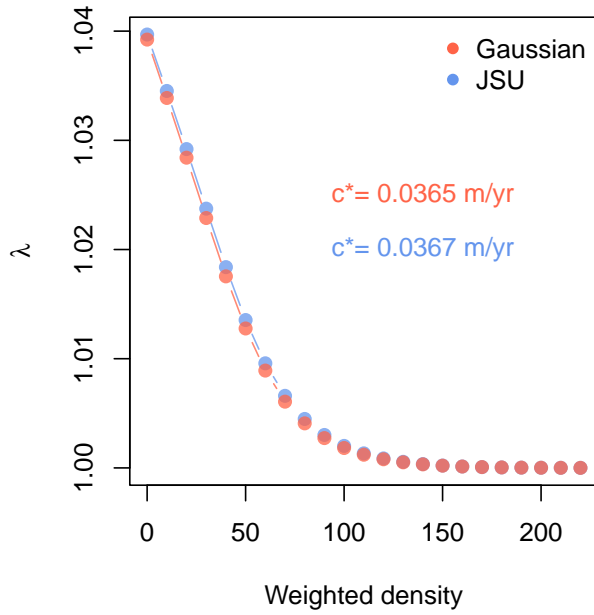


**Figure S-6:** Density dependence in fitness ( $\lambda$ ) and asymptotic velocity of the creosote encroachment wave ( $c^*$ ) for Gaussian and JSU growth kernels. Weighted density is the sum of sizes ( $\log(cm^3)$ ) of all conspecifics within a five-meter transect “window”. Figure made by script `creosote_growth_modeling_qgam.R`.

1156 established (mean remaining life expectancy of a median-sized shrub is 24,408 years)  
 1157 and its population growth and wave expansion are limited by very low seedling recruit-  
 1158 ment ((Drees et al., 2023)). Weak size-dependence in survival likely explains why the  
 1159 improvement in growth modeling had little influence on SIPM predictions.

1160 **S.4 Additional results**

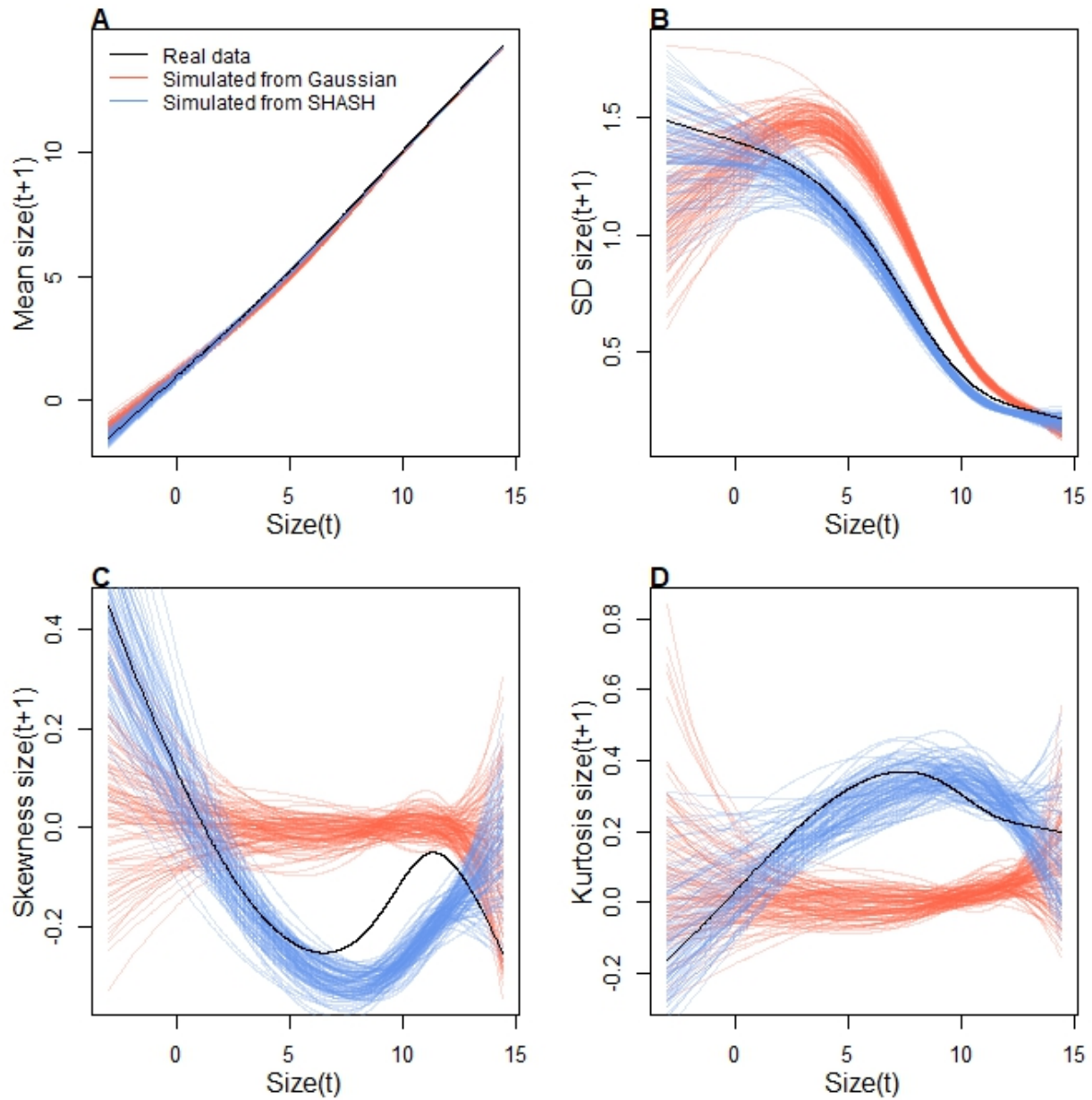


**Figure S-7:** Comparisons among real cactus data and data simulated from Gaussian and SHASH growth models for mean, standard deviation, NP skewness, and NP excess kurtosis of future size conditional on current size. Figure made by script `cactus_growth_modeling_qgam.R`.

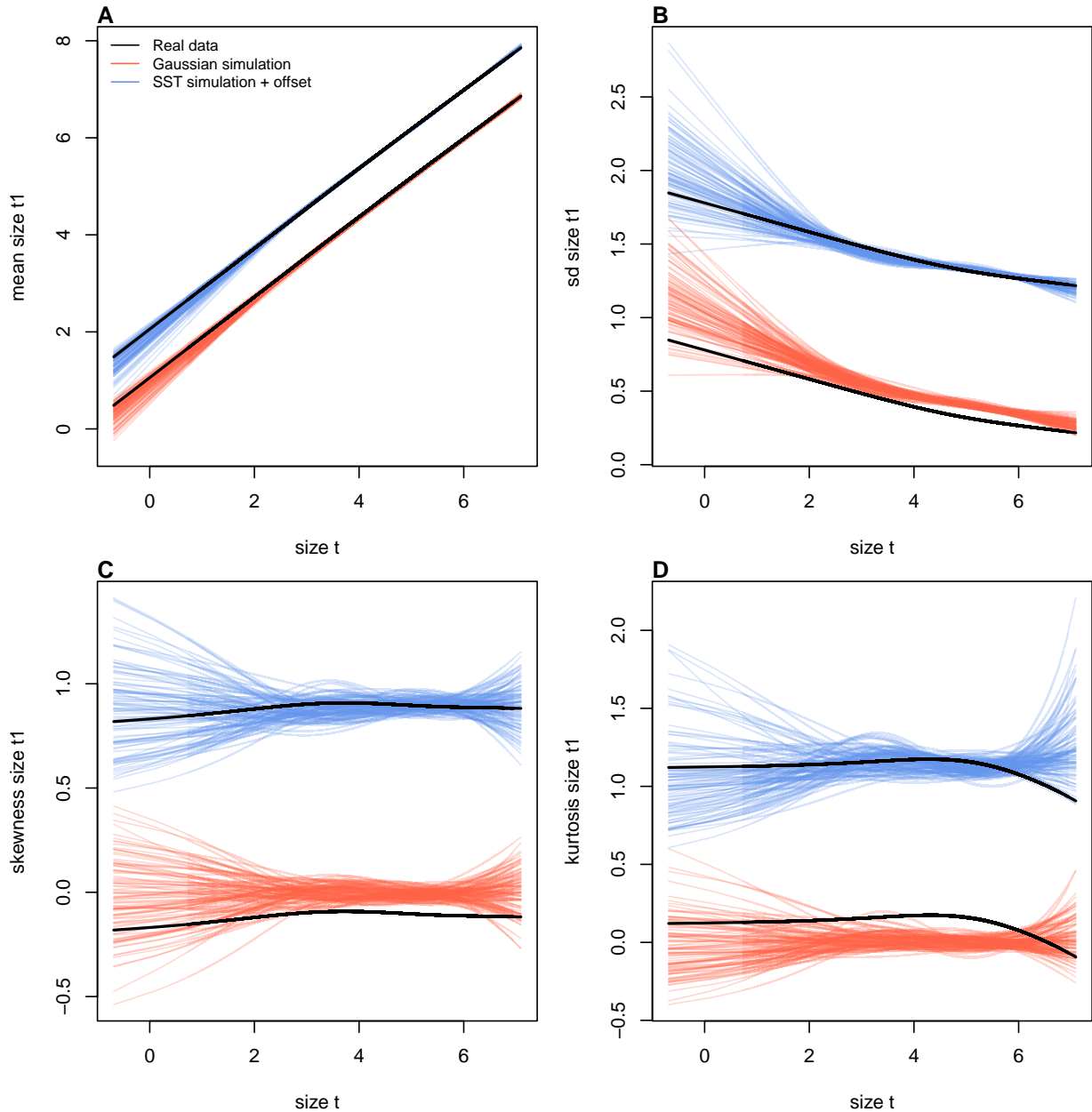


**Figure S-8:** Comparisons between real orchid data and data simulated from Gaussian and skewed  $t$  growth models for mean, standard deviation, NP skewness, and NP kurtosis of future size conditional on current size. Top row (A-D) shows plants that were vegetative at the start of the transition year and bottom row (E-H) shows plants that were flowering at the start of the transition year. Figure made by script `orchid_growth_modeling_rq.R`.